Clay minerals related to the circulation of geothermal fluids in boreholes at Rittershoffen (Alsace, France)

Jeanne Vidal, Patricia Patrier, Albert Genter, Daniel Beaufort, Chrystel Dezayes, Carole Glaas, Catherine Lerouge, Bernard Sanjuan

Clay minerals related to the circulation of geothermal fluids in boreholes at Rittershoffen (Alsace, France)

Jeanne Vidal [a],*, Patricia Patrier [b], Albert Genter [c], Daniel Beaufort [b], Chrystel Dezayes [d], Carole Glaas [c], Catherine Lerouge [d], Bernard Sanjuan [d]

[a] University of Strasbourg, CNRS UMR 7516 IPGS, 1 rue Blessig, F-67084 Strasbourg Cedex, France
[b] University of Poitiers, CNRS UMR 7285 IC2MP, HydrASA, Bat B8, Rue Albert Turpain, TSA51106, F-86073 Poitiers Cedex 9, France
[c] ES-Géothermie, 5 rue Lisbonne, 67300 Schiltigheim, France
[d] BRGM, 3 Av. Claude Guillemin, BP6009, 45060 Orléans Cedex 02, France

A B S T R A C T

Two geothermal wells, GRT-1 and GRT-2, were drilled into the granite at Rittershoffen (Alsace, France) in the Upper Rhine Graben to exploit geothermal resources at the sediment-basement interface. Brine circulation occurs in a permeable fracture network and leads to hydrothermal alteration of the host rocks. The goal of the study was to characterize the petrography and mineralogy of the altered rocks with respect to the permeable fracture zones in the granitic basement. As clay minerals are highly reactive to hydrothermal alteration, they can be used as indicators of present-day and paleo-circulation systems. Special attention has been paid to the textural, structural and chemical properties of these minerals. The fine-grained clay fraction ($<5\,\mu m$) was analyzed around the originally permeable fracture zones to observe the crystal structure of clay minerals using X-ray diffraction. Chemical microanalysis of the clay minerals was performed using scanning electron microscopy coupled with energy dispersive X-ray spectroscopy. The occurrences of mixed layers illite-smectite (~10% smectite) provide a promising guide for identifying the fracture zones that control the present-day circulation of geothermal fluids in the Rittershoffen wells. However, multistage paleo-circulation systems could lead to an abundance of heterogeneous and fine-grained illitic minerals that could plug the fracture system. The permeability of fracture zones in the GRT-1 well was likely reduced because of an intense illitization, and the well was stimulated. The occurrence of chlorite in the permeable fracture zones of GRT-2 is indicative of less intense illitization, and the natural permeability is much higher in GRT-2 than in GRT-1.

© 2017 The Authors. Published by Elsevier B.V. This is an open access article under the CC BY-NC-ND license (http://creativecommons.org/licenses/by-nc-nd/4.0/).

1. Introduction

In geothermal systems, alteration minerals provide useful information about the physico-chemical conditions of both past and present hydrothermal activity. This is particularly the case with clay minerals, which have been investigated as markers of circulation zones based on their reactivity to changes in physico-chemical conditions (Beaufort et al., 1992, 1996; Browne and Ellis, 1970; Flexser, 1991; Mas et al., 2006; Patrier et al., 1996; Reyes, 1990). The properties of clay minerals are affected by temperature in addition to several other factors, such as rock and fluid chemistries, time and the fluid/rock ratio. This study focused on the argillic alteration of permeable fracture zones related to a hydrothermal system located in the Upper Rhine Graben at Rittershoffen in France (Fig. 1). Two deep geothermal wells - GRT-1, which has a vertical trajectory, and GRT-2, which has a deviated trajectory - intersect natural, permeable fracture zones in the

sandstones and granitic basement beneath Rittershoffen (Baujard et al., 2017; Vidal et al., 2017). The influence of argillic alteration on the permeability of fracture zones at the borehole scale is an important milestone for an industrial project because fracture zones channel hot geothermal fluids that are exploited for high-temperature ($>160\,°C$) heat applications at the surface.

Geothermal systems are dynamic systems that are constantly evolving; thus, the observed secondary minerals potentially consist of several superimposed alteration assemblages. In Rittershoffen boreholes, the mineral products of the existing hydrothermal circulation system (160 °C) appear to be superimposed upon previous secondary minerals formed during earlier circulations events. Abundance of secondary minerals may lead to plugging and the transformation of fracture zones from conduits into barriers to fluid flow. As the nature of fracture permeability is an important aspect of this geothermal project, most of the cutting samples were collected along the open-hole sections of wells around the originally permeable (OP) fracture zones in both wells. Cutting samples from both GRT-1 and GRT-2 were investigated to identify the alteration mineralogies, and special attention was paid

* Corresponding author.
E-mail address: j.vidal@unistra.fr (J. Vidal).
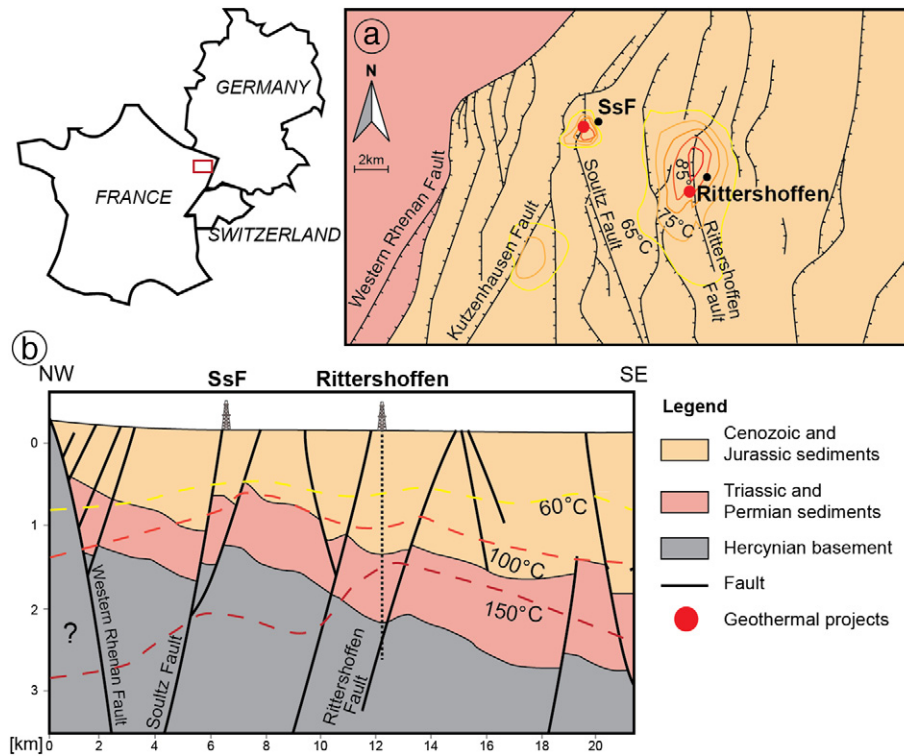
Fig. 1. Location of the Rittershoffen geothermal site. a) Geological and structural map of the Rittershoffen and Soultz-sous-Forêts (SsF) area. Isotherms at the top of the basement are from Baillieux et al. (2014). b) Geological cross section through the Rittershoffen and Soultz-sous-Forêts geothermal sites after *Geoportail of EU-Project GeORG - INTERREG IV Upper Rhine* (2012). The dashed line is an interpreted trajectory of the geothermal well GRT-1.

to the clay fraction. The fine-grained fraction of cuttings (<5 μm) was analyzed using X-ray Diffraction (XRD) to identify well-crystallized illite, poorly crystallized illite and mixed layers illite-smectite. Then, scanning electron microscopy (SEM) coupled with energy-dispersive X-ray spectroscopy (EDS) was used to analyze the chemical compositions of the clay minerals.

2. Geological context

The geothermal site at Rittershoffen is located in the Upper Rhine Graben (URG), approximately 15 km east of the Western Rhenan fault and less than 10 km from the well-known Soultz-sous-Forêts geothermal site (Alsace, France) (Fig. 1a). In the URG, the underground temperature distribution is spatially heterogeneous, and several geothermal anomalies are concentrated throughout the western side of the URG in the areas of Soultz-sous-Forêts and Rittershoffen (Baillieux et al., 2013; Pribnow and Schellschmidt, 2000; Schellschmidt and Clauser, 1996). Temperature anomalies at the top of the granitic basement indicated by several temperature measurements are concentrated along the Soultz and Kutzenhausen normal faults that dip toward the west (Fig.

1a) (Baillieux et al., 2014). These zones are attributed to the upwelling of hot geothermal fluids through fault zones within the crystalline basement and Triassic and Permian sandstones (Fig. 1b) (Benderitter et al., 1995; Pribnow and Clauser, 2000; Pribnow and Schellschmidt, 2000). Geothermal reservoirs in the granitic basement at Rittershoffen are quite similar to the reservoir at Soultz. Both deep fluids are of the NaCl type with total dissolved solids (TDS) values close to 100 g/L (Table 1) (Sanjuan et al., 2014, 2016). The pH values of the fluids in both reservoirs are close to 5.0. The fluids are interpreted as having originated from the mixing of primary marine brine with water of meteoric origin (Sanjuan et al., 2010, 2016). The estimated temperature of the deep reservoir calculated by primary cationic geothermometers (Na-K, Na-K-Ca, Na-K-Ca-Mg, K-Mg, Na-Li and Mg-Li) and by a $\delta^{18}O_{H2O-SO4}$ isotope geothermometer was 225 ± 25 °C at Soultz and at Rittershoffen (Sanjuan et al., 2016).

Alteration episodes of the granitic reservoir are well known to have occurred in deep wells at Soultz (Genter, 1989; Hooijkaas et al., 2006; Ledésert et al., 1999; Traineau et al., 1992). Early propylitic alteration of the whole granitic batholith is characterized by the formation of epidote, the partial transformation of primary biotite into Fe,Mg-chlorite

Table 1
Chemical compositions of geothermal fluid sampled in the Paleozoic granite at Soultz-sous-Forêts in the well GPK-2 at a measured depth of 5000 m (Sanjuan et al., 2014) and at Rittershoffen in the well GRT-1 at a measured depth of 2580 m (Sanjuan et al., 2016).

Location	T_{Bottom}	pH	TDS	Na	K	Ca	Mg	Cl	SO_4	SiO_2	Br	Li	Gas
	°C		g/L	mg/L	mg/L	mg/L	mg/L	mg/L	mg/L	mg/L	mg/L	mg/L	
Soultz-sous-Forêts	200	4.98	99	28,140	3195	7225	131	58,559	157	201	216	173	CO_2 N_2 CH_4
Rittershoffen	>160	6.27	101	28,451	3789	7200	138	59,900	220	146	251	190	unknown

and the partial replacement of primary potassic feldspar with small crystallites of illite. Then, hydrothermal alterations dominated by illite, quartz and calcite occur around fracture zones after fluid circulations. Several alteration facies were identified by Hooijkaas et al. (2006). The same granitic batholith was encountered at Rittershoffen. As geothermal fluids are similar, alterations observed at Soultz could be a reasonable reference for petrographical studies at Rittershoffen.

3. OP fracture zones, thermal profile and hydraulic yield of the geothermal wells at Rittershoffen

At Rittershoffen, two wells, GRT-1 and GRT-2, penetrate the Cenozoic, Mesozoic and Permian sediments overlying the Paleozoic basement. The wells were drilled to a true vertical depth of 2.6 km in the southeastern end of a horst and targeted the so-called Rittershoffen normal fault at the top of the basement (Baujard et al., 2017). Based on a seismic reflection interpretation of the sedimentary cover, this fault strikes N-S, dips 45° westward and displays an apparent vertical offset of approximately 200 m (Fig. 1b) (Baujard et al., 2017). Wells intersect the fracture network associated with the Rittershoffen fault in Buntsandstein and

Permian sandstones (from ~245 Ma to ~255 Ma) and in the Carboniferous granite (~340 Ma) (Baujard et al., 2017). The fracture network was investigated in the open-hole sections using acoustic image logs correlated with standard geophysical logs (e.g., gamma ray, neutron porosity), cutting observations and permeability indicators (i.e., mud losses, gas occurrences), and temperature logs (Vidal et al., 2017). If fracture zones present indications of permeability or temperature anomalies at the borehole scale after drilling operations without any stimulation operations, they are qualified as OP fracture zones (Vidal et al., 2017). In GRT-1, one main OP fracture zone was observed in the granitic basement from measured depths (MD) of 2325 to 2368 m (Fig. 2) (Vidal et al., 2016a, 2017). In GRT-2, four OP fractures zones were observed in the granitic basement (Fig. 3) (Baujard et al., 2017; Vidal et al., 2017). The main OP fracture zone is located at 2766–2800 m MD (Fig. 3). Others OP fracture zones are located at approximately 2535 m MD, approximately 2950 m MD and approximately 3050 m MD (Vidal et al., 2017).

The thermal profiles of two wells are divided into two parts (Baujard et al., 2017).

- The uppermost part is associated with a linear geothermal gradient of 95 °C/km indicative of conductive heat transfer (Baujard et al., 2017).
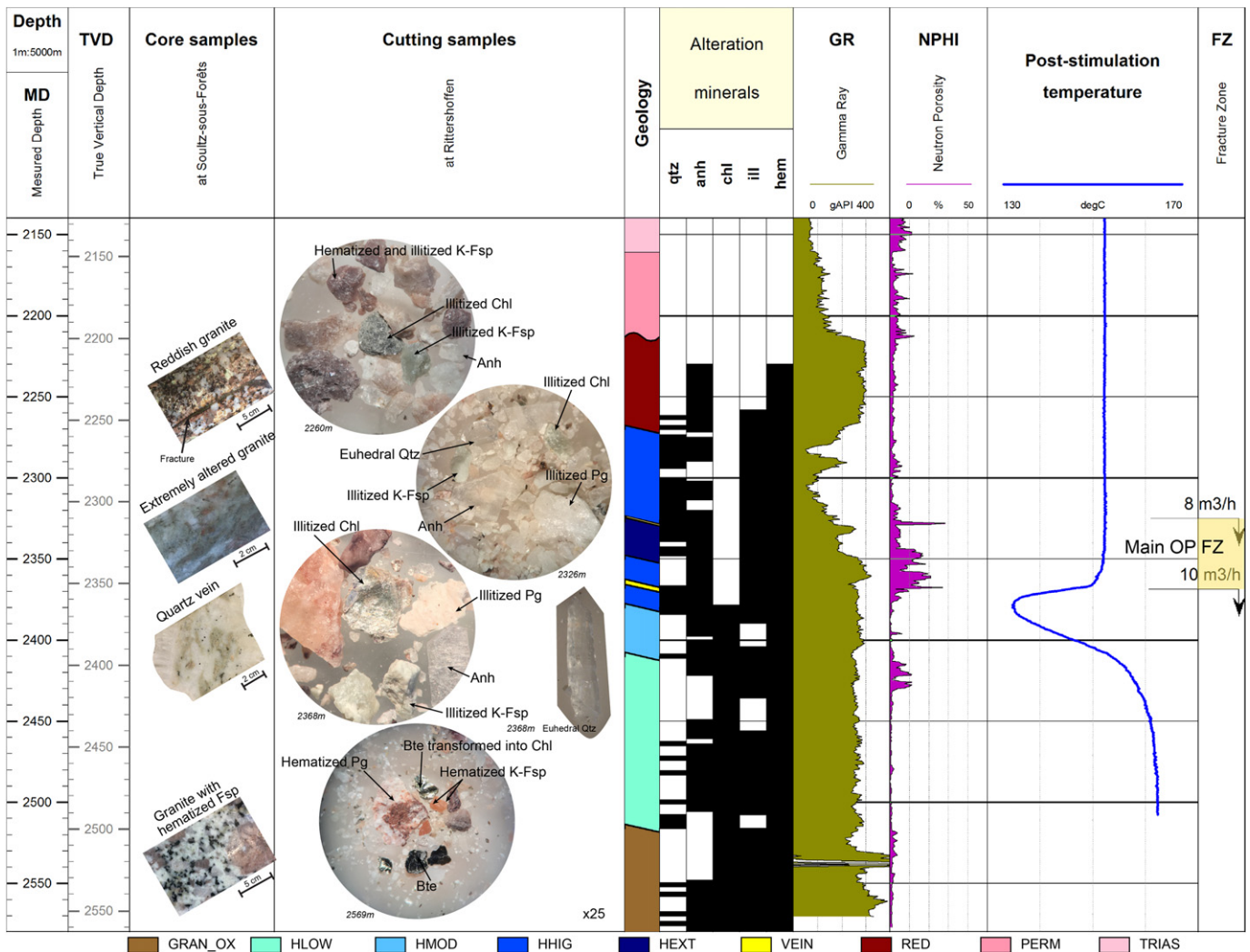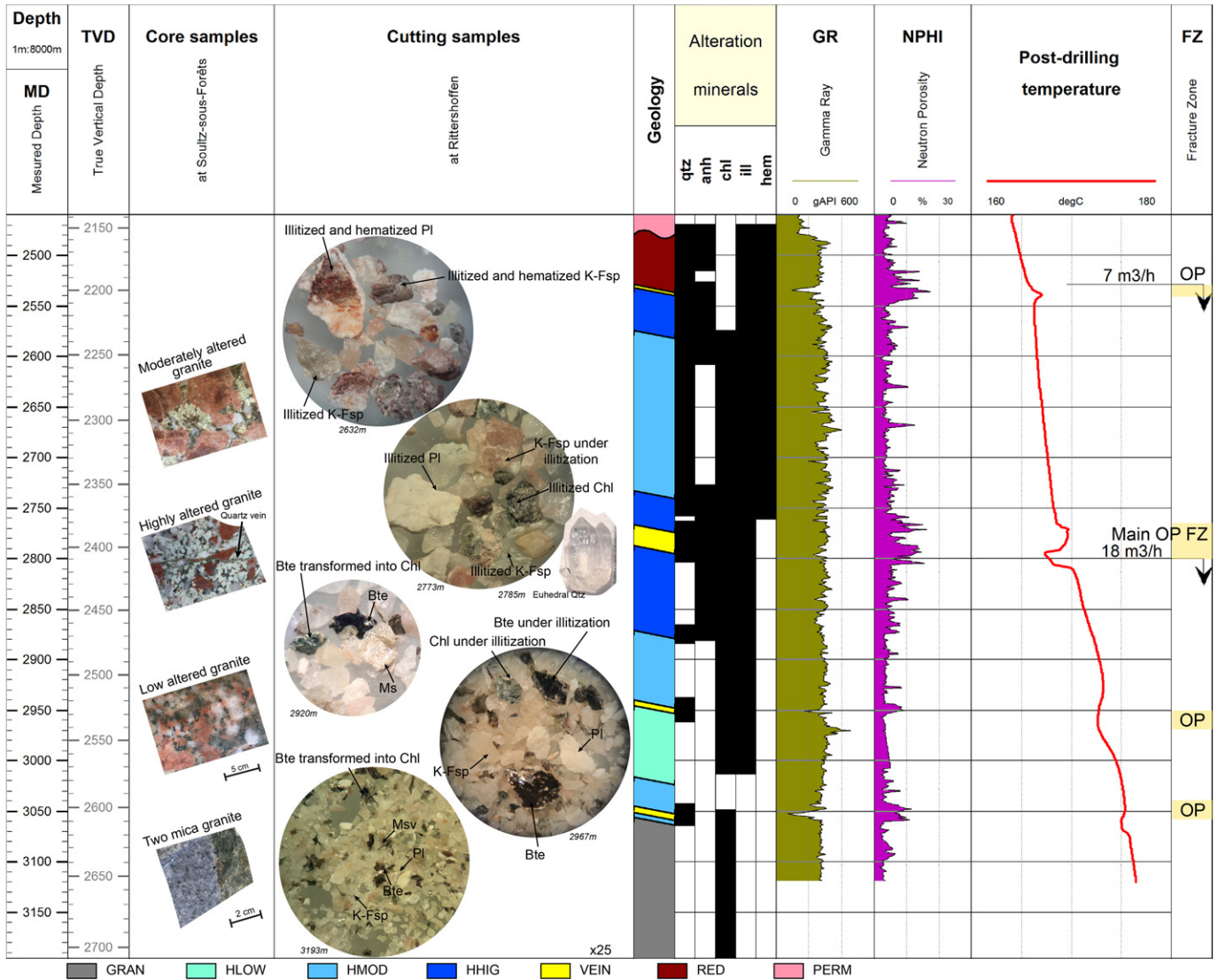

Fig. 2. Temperature log in the granitic basement of GRT-1 correlated with cutting sample observations, occurrences of alteration minerals, and gamma ray (GR) and neutron porosity (NPHI) data. The light-yellow interval is an originally permeable (OP) fracture zone identified from a structural analysis (Vidal et al., 2016a, 2017). Core samples from Soultz-sous-Forêts are indicated as potential analogs of the alteration grades observed in the cuttings. Black in the alteration mineral columns indicates the presence of the minerals in cuttings. Cuttings observed with a hand lens are magnified 25×. Qtz = quartz, anh = anhydrite, chl = chlorite, ill = illite, hem = hematite, bte = biotite, pg = plagioclase feldspar, K-Fsp = potassic feldspar. GRAN_OX = propylitic alteration and hematite precipitation, HLOW = low degree of argilization, HMOD = moderate degree of argilization, HHIG = high degree of argilization, HEXT = extreme degree of argilization, VEIN = quartz vein, RED = reddish granite affected by paleoweathering, PERM = Permian sediments, TRIAS = Triassic sediments.

Fig. 3. Temperature log in the granitic basement of GRT-2 correlated with cutting sample observations, occurrences of alteration minerals, and gamma ray (GR) and neutron porosity (NPHI) data. Light-yellow intervals are originally permeable (OP) fracture zones identified from a structural analysis (Vidal et al., 2017). Core samples from Soultz-sous-Forêts are indicated as potential analogs of the alteration grades observed in the cuttings. Black in the alteration mineral columns indicates the presence of the minerals. Cuttings observed with a hand lens are magnified 25×. Qtz = quartz, anh = anhydrite, chl = chlorite, ill = illite, hem = hematite, bte = biotite, pg = plagioclase feldspar, K-Fsp = potassic feldspar, ms = muscovite. GRAN = propylitic alteration, HLOW = low degree of argilization, HMOD = moderate degree of argilization, HHIG = high degree of argilization, VEIN = quartz vein, RED = reddish granite affected by paleoweathering, PERM = Permian sediments.

The sedimentary formations from the Cenozoic and Mesozoic (Lower Jurassic and Upper Triassic) may serve as cap rocks that insulate the active hydrothermal system below.

• The deepest part exhibits a null geothermal gradient in GRT-1 (Fig. 2) and a low geothermal gradient of 18 °C/km in GRT-2 (Fig. 3) (Baujard et al., 2017). Heat and matter transfer in these hard, fractured sandstones (of the Buntsandstein and the Permian formations) and the fractured granitic basement are dominated by convective processes. This section has positive and negative deviations from the geothermal gradient, which are positive or negative anomalies interpreted as the thermal signature of the OP fracture zones (Baujard et al., 2017; Vidal et al., 2017). Each OP fracture zone is associated with thermal anomalies that may be caused by the outflow of hot geothermal fluids (positive anomalies) or by remnant cooling of porous damage zones after mud invasion during drilling operations and the massive injection of water during stimulation operations (negative anomalies) (Barton et al., 1995; Bradford et al., 2013; Davatzes and Hickman, 2005; Genter et al., 2010; Vidal et al., 2017).

The bottom-hole temperatures are 166 °C in GRT-1 and 177 °C in GRT-2 (Baujard et al., 2017). The hydraulic behavior of the vertical well GRT-1 is controlled by the main OP fracture zone in the granitic basement from 2325 to 2368 m MD (Fig. 2), and its natural permeability was deemed too low for industrial exploitation (Baujard et al., 2017; Vidal et al., 2016a). The well was thermally, chemically and hydraulically (TCH) stimulated with success, and its hydraulic yield was enhanced from 0.5 L/s/bar to 2.5 L/s/bar (Baujard et al., 2017). The hydraulic behavior of the deviated well GRT-2 is controlled by several OP fracture zones. The natural permeability of the well was high enough for industrial exploitation and presented a good hydraulic yield (higher than 3 L/s/bar) and therefore was not stimulated (Baujard et al., 2017). These OP fracture zones in the granitic basement host the fracture-controlled circulation of fluids that generate the observed hydrothermal alterations. The study focused on the hydrothermal alteration in the granitic basement inferred from observations of clay minerals. Associated minerals such as silicates (i.e., quartz and other forms of silica) and carbonates also provide information about the hydrothermal alteration, but they were not part of the study.

4. Methodology

4.1. Evaluation of argilization from observations of cutting

The first part of the study involved the investigation of the alteration petrography of the cutting samples by hand-lens examination at 3-m depth intervals. With cutting samples, spatial resolution is low and textural relations between minerals are not studied. Moreover, minerals from the fractures and the surrounding granitic protolith are commonly mixed within each cutting sample. The degree of argilization of the primary minerals and the occurrence of chlorite were investigated by hand-lens examination of the granitic samples. The degrees of alteration of the granitic cuttings were determined based on observations of analogue core samples from Soultz (core samples in Figs. 2 and 3) (Genter and Traineau, 1992; Hooijkaas et al., 2006). The whole granitic basement affected by propylitic alteration is designated GRAN (core sample in Fig. 3). The top of the granitic basement is affected by paleo-weathering related to Permian exhumation of the basement. This facies is associated with hematization and designated reddish granite (RED) (core sample in Fig. 2). Moreover, four types of granitic facies were determined to show increasing levels of argilization of the primary minerals:

- A facies with a low degree of argilization (HLOW) is characterized by the persistence of weakly argilized biotite and chlorite and by unaltered plagioclase and potassic feldspars. The texture of the granitic protolith is preserved (core sample in Fig. 3);
- A facies with a moderate degree of argilization (HMOD) is characterized by the total argilization of biotite and the preservation of unaltered plagioclase and potassic feldspars (core sample in Fig. 3);
- A facies with a high degree of argilization (HHIG) is characterized by the total argilization of biotite and the partial to total replacement of plagioclase and potassic feldspars with clay minerals (core samples in Fig. 3);
- A facies with an extremely high degree of argilization (HEXT) is characterized by the total argilization of primary minerals (i.e., biotite and the plagioclase and potassic feldspars). The overall texture of the core sample is completely modified compared with that of the granitic protolith (core samples in Fig. 2).

The macroscopic observations were correlated with the geophysical logs (i.e., gamma ray and neutron porosity) to provide supplementary information about the vertical distribution of the clay minerals identified in the cuttings. The gamma ray log involves the measurement of the potassium, thorium and uranium contents used to detect the leaching of radioactive primary minerals (negative anomaly) or the presence of clay minerals that incorporate radioactive chemical elements within the fracture zones (positive anomaly). The neutron porosity log is based on the response of a formation to the emission of fast neutrons by a given source; in granite, that response is positive if there is a fracture or if clays and hydrated minerals occur in the formation.

Then, thin sections made from mount cuttings in epoxy were observed by microscopy in approximately fifty cutting samples from both wells. The degree of illitization of the primary minerals was estimated from microscopic observations of the replacement rate of the K-feldspars by illite in thin sections.

4.2. Identification of clay minerals

The second part of the study focused on the identification of clay minerals. Twenty-one and thirty-eight cuttings samples were collected from GRT-1 and GRT-2, respectively. The sampling was concentrated in the permeable and altered fracture zones, which were identified within the granitic basement using acoustic image and temperature logs. Some of the samples were located in lightly altered zones and were used as reference materials, as they are believed to be representative of rocks preserved from present-day fluid circulation properties. Samples were not ground; they were dispersed in distilled water by ultrasonic vibration to disintegrate the particles. Oriented powders on glass slides were prepared with a < 5 μm clay suspension, obtained by sedimentation. Clay minerals were identified by XRD of air-dried and ethylene–glycol (EG)-saturated oriented powders carried out on a Bruker D8 Advance diffractometer (CuKα radiation, 40 kV, 40 mA). The analytical conditions were as follows: angular domain: 2.5–30° 2θ; step increment: 0.025 2θ; and counting time per step: 3 s. XRD data acquisition and treatment were conducted using the X'Pert HighScore software (PANalytical B.V.). The clay minerals were identified according to the literature (Brindley and Brown, 1980) (Fig. 4). When present, the (001) reflection from the illitic minerals was deconvolved into poorly crystallized illite (PCI), well-crystallized illite (WCI) and ordered illite-rich mixed layered illite/smectite (I/S) using the Fityk software (Fig. 4c). The full width at half maximum (FWHM) intensity of the typical (001) reflections of WCI and PCI at 10 Å is a good indicator of the crystallinity along the c axis (Kubler, 1968). The crystallinity along the c axis of the chlorite was estimated from the FWHM intensity of the (002) reflection at 7 Å.
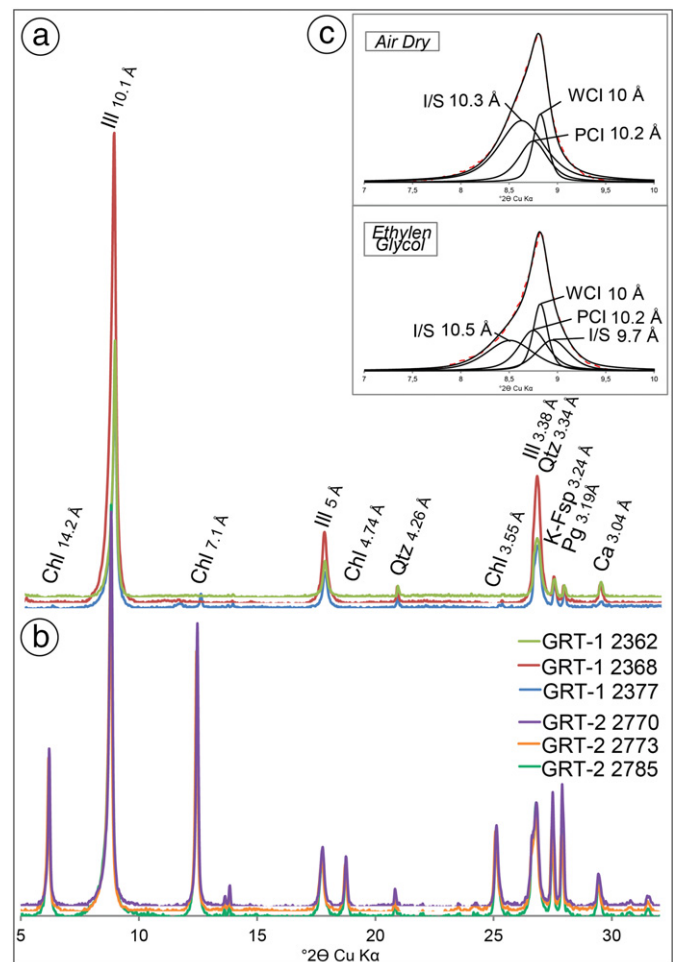
Fig. 4. X-ray diffractograms of the clay fraction as observed in the main OP FZ a) in GRT-1 (samples 2362, 2368 and 2377) and b) in GRT-2 (samples 2770, 2773 and 2785). Ill = illite, Chl = chlorite, Qtz = quartz, Pg = plagioclase feldspar, K-Fsp = potassic feldspar, Ca = calcite. c) deconvolution of the 7–10° 2Θ CuKα domain of the X-ray diffractograms (<5 μm clay fraction) of air-dried and EG-saturated oriented powder of an example sample. I/S: ordered illite/smectite mixed layer; WCI: well-crystallized illite, PCI: poorly crystallized illite. Dashed red line represents the data.

4.3. Analysis of chemical composition of clay minerals

Finally, the third part of the study involved the investigation of the chemical compositions of clay minerals using a JEOL 5600LV SEM, which was equipped with a BRUKER XFlash 4030 Silicon Drift Detector (accompanied by the SPIRIT software). The analytical conditions were as follows: 15 kV; 1 nA; counting time: 60 s; and working distance: 16.5 mm. The analyzed elements were Si, Al, Fe, Mg, Mn, Ti, Ca, Na
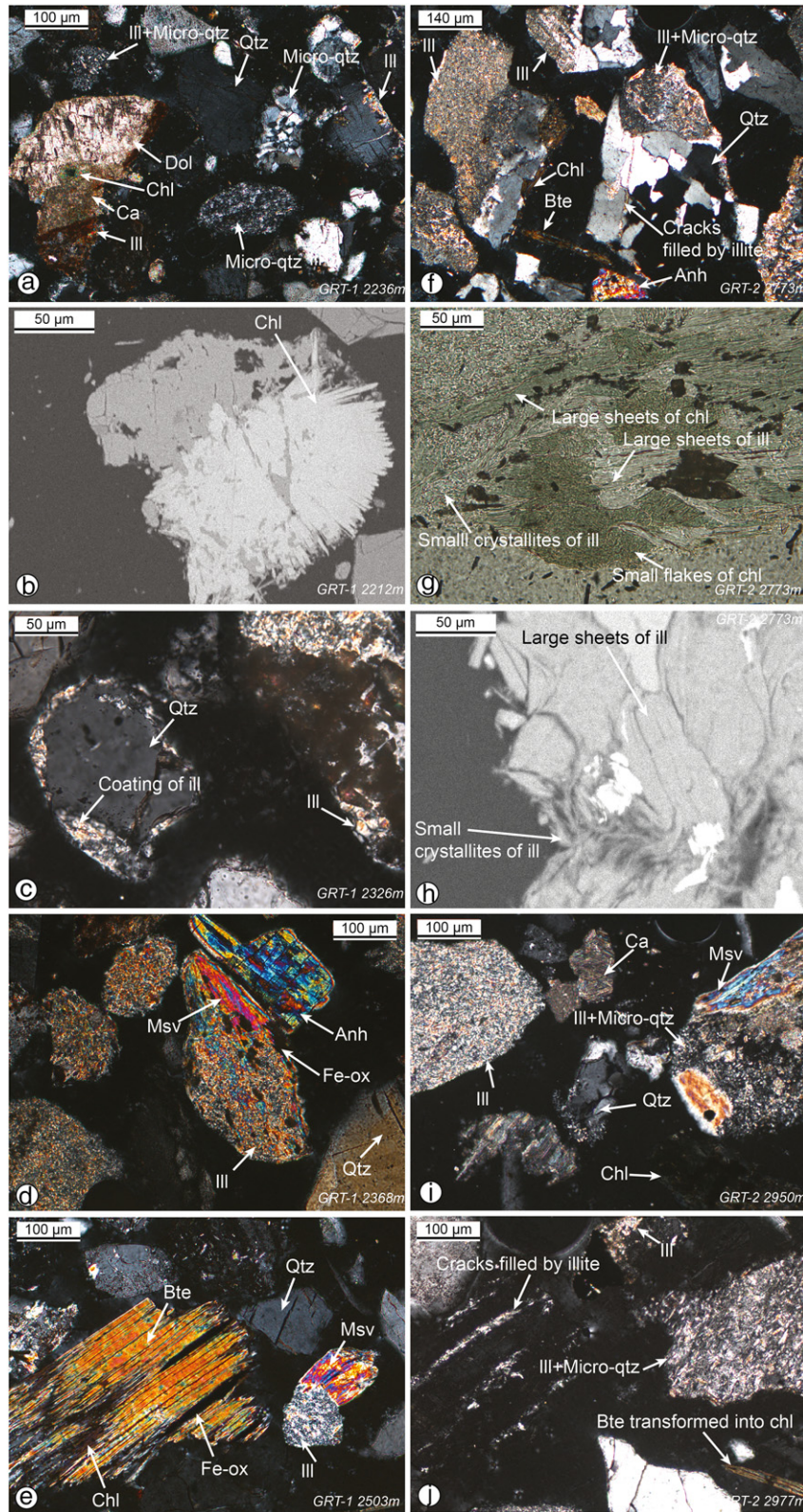
Fig. 5. Microscopic observations of thin sections of cuttings fixed in epoxy in GRT-1 at a) 2236 m MD (PPL), b) 2212 m MD (SEM observations), c) 2326 m MD (PPL), d) 2368 m MD (PPL), and e) 2503 m MD (plane polarized light, PPL); and in GRT-2 at f) 2773 m MD (PPL), g) 2773 m MD (crossed polarized light, XPL), h) 2273 m MD (SEM), i) 2950 m MD (PPL) and j) 2977 m MD (PPL) Qtz = quartz, Bte = biotite, Chl = chlorite, Ill = illite, Py = pyrite, Anh = anhydrite, Dol = dolomite, Ca = calcite, Fe-ox = iron oxides.

and K. The system was calibrated with a variety of synthetic oxide and natural silicate standards. The reproducibilities of the standard analyses were approximately 1%, except for Na, which had a reproducibility of 1.5%.

5. Alteration petrography in the geothermal wells at Rittershoffen

5.1. Observations in GRT-1

The top of the granitic basement is encountered at 2212 m MD in GRT-1. The first granitic facies intersected is the RED facies down to 2270 m MD (Fig. 2). Cuttings near the contact with the overlying sediments are reddish because of the intense precipitation of hematite (cuttings in Fig. 2). Fractures into reddish granite contain a large amount of illitic minerals associated with micro-quartz (Fig. 5a). Carbonates such as calcite and dolomite as well as sulfate are prevalent in fractures. Some green chlorite minerals are observed (Fig. 5a). More microscopy images of the cutting samples in GRT-1 are provided in the Supplementary material S1. SEM observations indicate epitaxial growth of the large chlorite (>50 μm) that likely crystallized from hydrothermal circulations (Fig. 5b). The RED facies is correlated with a well-known pattern of gamma rays that is characteristic of the reddish granite in the area (Fig. 2) (Vidal et al., 2016b). At the top of the granitic basement, the gamma ray intensity decreases abruptly in the sedimentary cover.

Below the RED facies, an HHIG facies is intersected down to 2326 m MD (cuttings in Fig. 3).

The main OP fracture zone presents abundant euhedral quartz from 2326 to 2329 m MD and from 2365 to 2368 m MD that could indicate the presence of quartz veins (cuttings in Fig. 2). These quartz veins are associated with a sharply negative anomaly of gamma ray radiation (Fig. 2) and have already been observed in acoustic image logs (Vidal et al., 2017). Small crystallites of illitic minerals occur as grain coatings of quartz (Fig. 5c). At the top of the main OP fracture zone, a HEXT facies is observed from 2329 to 2350 m MD (Fig. 2) in which cuttings are highly bleached in response to intense hydrothermal alteration (cuttings in Fig. 2). Anhydrite and pyrite are abundant in the main OP fracture zone of GRT-1. Chlorite is seldom observed within the main OP fracture zone of GRT-1. At the bottom of the main OP fracture zone, an HHIG facies is observed down to 2380 m MD (cuttings in Fig. 2), and primary biotite and local feldspars are completely replaced by small crystallites of illitic minerals (Fig. 5d). Neutron porosity values confirm the significant argilization of the main OP fracture zone, with values between 10 and 20% from 2340 to 2370 m MD and maxima of nearly 40% at 2325 and 2370 m MD.

Below the main OP fracture zone, from 2380 to 2410 m MD, an HMOD facies is encountered, and then from 2410 to 2516 m MD, an HLOW facies is observed (Fig. 2). The deep granitic samples from 2516 to 2580 m MD are affected by propylitic alteration with the partial transformation of primary biotite into chlorite and the partial replacement of primary potassic feldspar or muscovite with small crystallites of illitic minerals (Fig. 5e). Cuttings exhibit a reddish colour, and this facies is designated GRAN_OX (Fig. 2).

5.2. Observations in GRT-2

The top of the granitic basement is encountered at 2480 m MD in GRT-2. The first granitic facies is RED down to 2533 m MD (Fig. 3). At the base of the RED facies, the abundance of euhedral quartz from 2533 to 2536 m MD suggests the presence of quartz veins associated with the presence of an OP fracture zone at the same depth. Then, an HHIG facies is observed from 2536 to 2578 m MD, and an HMOD facies is observed from 2578 m MD to 2737 m MD (Fig. 3).

The main OP fracture zone in GRT-2 is associated with an HHIG facies observed from 2737 to 2875 m MD. The top of the main OP fracture zone is associated with neutron porosity values between 10% and 20% from 2760 to 2810 m MD, which are correlated with the significant

argilization of the cuttings (Fig. 3). In thin sections, primary minerals are replaced by illitic minerals but are still identifiable compared with the main OP fracture zone in GRT-1 (Fig. 5f). The microscopic observations indicate at least two different sizes of illitic minerals that are likely associated with different hydrothermal events. Illitic minerals are present as large sheets (>50 μm) as well as small crystallites (<5 μm) and are sometimes present as the infill of cracks (Fig. 5f, g and h). At least two sizes of chlorite are also observed. Chlorite derived from the transformation of biotite is observed as large sheets (>50 μm), and another population of chlorite in the form of small flakes (<5 μm) is also observed (Fig. 5h). More microscopy images of the cutting samples in GRT-2 are provided in the Supplementary material S2. In the main OP fracture zone, cuttings from 2770 to 2791 m MD indicate euhedral quartz, which is interpreted as the occurrence of quartz veins (Fig. 3). These cuttings correlate with quartz veins observed in acoustic image logs (Vidal et al., 2017).

Below the main OP fracture zone, an HMOD facies is observed until the OP fracture zone at 2944 m MD. Locally, primary minerals are completely transformed into small crystallites of illitic minerals, while primary muscovite could be preserved (Fig. 5i). Green chlorite and calcite are also found at these depths. The OP fracture zone is associated with an abundance of euhedral quartz from 2944 to 2950 m MD correlated with a sharply negative anomaly of gamma ray radiation (Fig. 3). Below the OP fracture zone, from 2950 to 3020 m MD, an HLOW facies is associated with primary quartz minerals intersected by microcracks filled with illitic minerals or with an assemblage of microquartz and illitic minerals (Fig. 5j). Then, the increase in neutron porosity until 13% suggests an increase in the argilization of cuttings. Cuttings from 3020 to 3046 m MD confirm this increase in argilization and are associated with an HMOD facies (Fig. 3). The deepest OP fracture zone is associated with an abundance of euhedral quartz from 3046 to 3061 m MD correlated with a sharp negative anomaly of gamma ray radiation (Fig. 3). The deepest cuttings, from 3061 to 3196 m MD, are light gray (Fig. 3). They are associated with the propylitic alteration and are designated GRAN.

In conclusion, four main facies of argilization were observed in GRT-1, and three were observed in GRT-2 (Figs. 2 and 3 and Supplementary material 3). An HEXT facies is not observed in the main OP fracture zones of GRT-2, the primary minerals are not completely transformed into illitic minerals in the OP fracture zones of GRT-1, and Fe-rich chlorite is much more abundant. The highest levels of alteration (HHIG and HEXT) are observed in the main OP fractures zones of GRT-1 and GRT-2 (Figs. 2 and 3 and Supplementary material 3). Euhedral quartz is always observed in abundance within the OP fracture zones.

6. Identification of clay minerals

X-ray diffractograms indicate that the clay alteration products are dominated by illite and chlorite in the Rittershoffen wells (Fig. 4). The (001) reflections of the illitic minerals at 10 Å are complex. The (001) reflections were deconvolved into two or three Gaussian peaks (Fig. 4c). Two peaks that correspond to the index peaks of WCI and PCI are consistently observed at approximately 10 Å and 10.2 Å, respectively (Fig. 4c). The WCI peak corresponds to a d-value of 10 Å and is characterized by a narrow FWMH that ranges from 0.08 to 0.24°2θ in GRT-1 and from 0.09 to 0.18°2θ in GRT-2. The PCI peak corresponds to a d-value of 10.2 Å and is characterized by a broader FWMH (between 0.26 and 0.48°2θ in GRT-1 and between 0.18 and 0.44°2θ in GRT-2). Microscopic observations reveal that illitic minerals occur as large sheets and as small crystallites. Deconvolution is therefore based on a first-order approximation with well-crystallized illitic minerals and poorly crystallized illitic minerals. However, there are likely more illitic populations.

Mixed layers I/S (~10% smectite) were identified in some of the samples. In air-dried samples, the layers are characterized by a broad peak near 10.3 Å that splits into two peaks near 10.5 Å and 9.7 Å after EG

saturation (Fig. 4c) (Lanson et al., 1995). The WCI and PCI peaks do not shift after EG saturation. Chlorites were identified by their non-expandability and their harmonic peaks at 14 Å and 7 Å. The FWHM of the peak at 7 Å varies between 0.08 and 0.12°2θ in GRT-1 and between 0.09 and 0.18°2θ in GRT-2. Chlorite is less abundant in the diffractograms of GRT-1 than in those of GRT-2 (Fig. 4).

6.1. Observations in GRT-1

Based on the crystallographic properties of the illitic minerals, two zones can be observed in the granite (Fig. 6a).

The shallowest zone is composed of samples from 2212 to 2338 m MD that are associated with the first three alteration facies intersected by the well GRT-1, RED, HHIG and HEXT. In this zone, the average proportion of WCI (%Int WCI) is 0.43, and the average FWHM of WCI is 0.15°2θ. The average proportion of PCI (%Int PCI) is 0.31, and the average

FWMH of PCI is 0.34°2θ. Mixed layers I/S are systematically present in this section, with an average %Int I/S of 0.26.

The deepest zone is composed of samples from 2347 to 2503 m MD that are associated with the last three alteration facies intersected by the well GRT-1, HHIG, HMOD and HLOW. In this zone, the %Int WCI is 0.72, and the average FWHM of WCI is 0.15°2θ. The average %Int PCI is 0.40, and the average FWMH of PCI is 0.28°2θ. Mixed layers I/S layers are no longer present in this section.

The crystallographic properties of chlorite are more strongly influenced by the main OP fracture zone than by the limits of alteration facies, as observed for illitic minerals (Fig. 6a).

From the top of the granitic basement (2212 m MD) to the top of the main OP fracture zone (2326 m MD), the average proportion of chlorite (%Int Chl) is 0.05 (Fig. 6a). Chlorite is only observed in one sample of the main OP fracture zone at 2354 m MD, wherein the highest proportion of chlorite in GRT-1 (0.97) is observed. From the base of the main OP
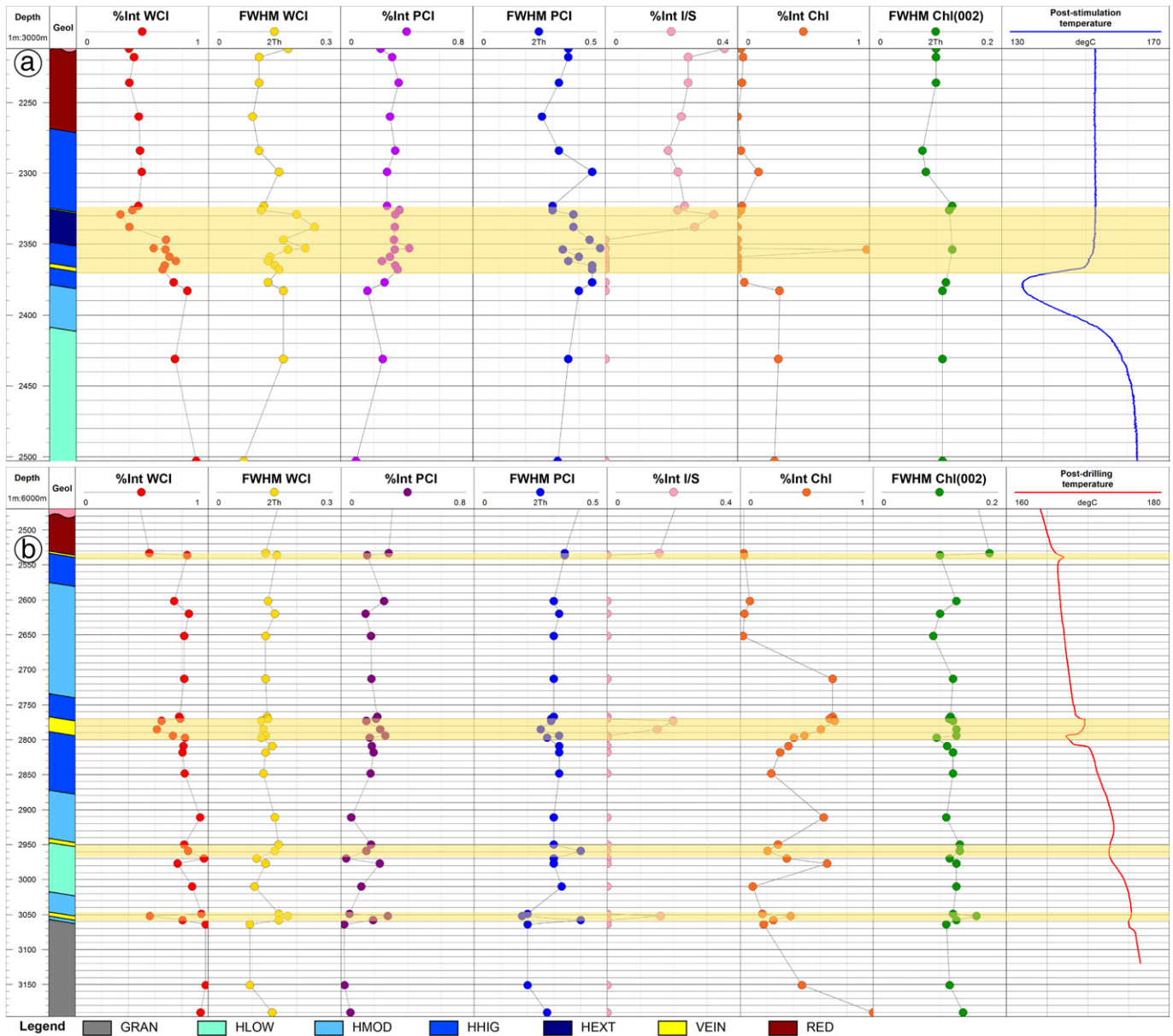

Fig. 6. Crystal structure properties of the illitic minerals and chlorite measured using XRD of the <5 μm clay fraction versus depth a) in GRT-1 and b) in GRT-1. Relative proportion of WCI: %Int WCI = WCI int/(WCI int + PCI int + I/S int), where WCI int = the intensity of the peak deconvolved from the (001) reflection of the illitic minerals. Relative proportion of Chl: %Int Chl = (Chl int/(Chl int + WCI int + PCI int + I/S int), where Chl int = the intensity of the peak of the (002) reflection of the chlorite. Light-yellow intervals represent originally permeable (OP) fracture zones from a structural analysis (Vidal et al., 2017, 2016a).

fracture zone (2377 m MD) to the bottom of the granitic basement (2503 m MD), chlorite is observed with an average %Int Chl of 0.24. With an average value of 0.10°2θ, the FWHM values of chlorite do not vary significantly with depth.

6.2. Observations in GRT-2

The crystallographic properties of illitic minerals are more strongly influenced by the occurrence of the OP fracture zone than by limits of alteration facies, as observed for GRT-1 (Fig. 6b).

From the top of the granitic basement (2480 m MD) to the bottom of the granitic basement (3196 m MD), %Int WCI tends to increase with depth (Fig. 6b). The average %Int WCI is 0.78, with an average FWMH of 0.13°2θ. Locally, the %Int WCI decreases in OP fracture zones:

- %Int WCI is 0.56 for the sample at 2533 m MD;
- %Int WCI is 0.65 and 0.61 for samples at 2773 and 2785 m MD;
- %Int WCI is 0.56 for the sample at 3052 m MD.

From the top of the granitic basement (2480 m MD) to the bottom of the granitic basement (3196 m MD), %Int PCI tends to decrease with depth (Fig. 6b). The average %Int PCI is 0.16, with an average FWMH of 0.30°2θ. Locally, %Int PCI increases at each OP fracture zones:

- %Int PCI is 0.29 for the sample at 2533 m MD;
- %Int PCI is 0.23 and 0.27 for samples at 2785 and 2794 m MD;
- %Int PCI is 0.18 and 0.15 for samples at 2950 and 2959 m MD;
- %Int WCI is 0.28 for the sample at 3052 m MD.

Mixed layers I/S are observed in samples at 2533, 2773, 2785 and 3052 m MD and are associated with OP fracture zones (Fig. 6b). Outside OP fracture zones, mixed layers I/S are no longer observed.

Chlorite is observed in all samples from the granitic basement of GRT-2 (Fig. 6b). The average %Int Chl is 0.38, and the FWHM is relatively constant, with an average value of 0.12°2θ (Fig. 6b). In the main OP fracture zone, the %Int Chl decreases from 0.71 at 2773 m MD to 0.23 at 2848 m MD.

In conclusion, the granitic basement is characterized by a general increase in %Int WCI and a decrease in %Int PCI with depth. However, local variations are associated with OP fracture zones in both wells. Each OP fracture zone is associated with a decrease in %Int WCI, an increase in %Int PCI and the occurrences of mixed layers I/S. These variations are more strongly correlated with the alteration facies limit in GRT-1 than in GRT-2. In GRT-1, the main OP fracture zone appears to act as an interface between two zones that are quite distinct, with occurrences of mixed layers I/S above and no longer mixed layers I/S below.

7. Chemical compositions of clay minerals

The structural formulae of the illitic minerals were calculated relative to a structure containing 11 oxygen atoms and assuming that the total iron content was composed of Fe^{3+} (Supplementary material 4). The structural formulae of the chloritic minerals were calculated relative to a structure containing 14 oxygen atoms and assuming the total iron content was composed of Fe^{2+} (Supplementary material 4).

7.1. Observations in GRT-1

The chemical analyses of the illitic minerals (WCI + PCI + ml I/S) in GRT-1 do not demonstrate major variations with depth (Fig. 7a). The interlayer charge is between 0.83 and 0.90, and the average octahedral Al content is 1.67 ± 0.05 per $O_{10}(OH)$ (Supplementary material 4). Samples above the main OP fracture zone (i.e. from 2212 to 2329 m MD) present an XFe ratio < 0.5, whereas samples in the main OP fracture
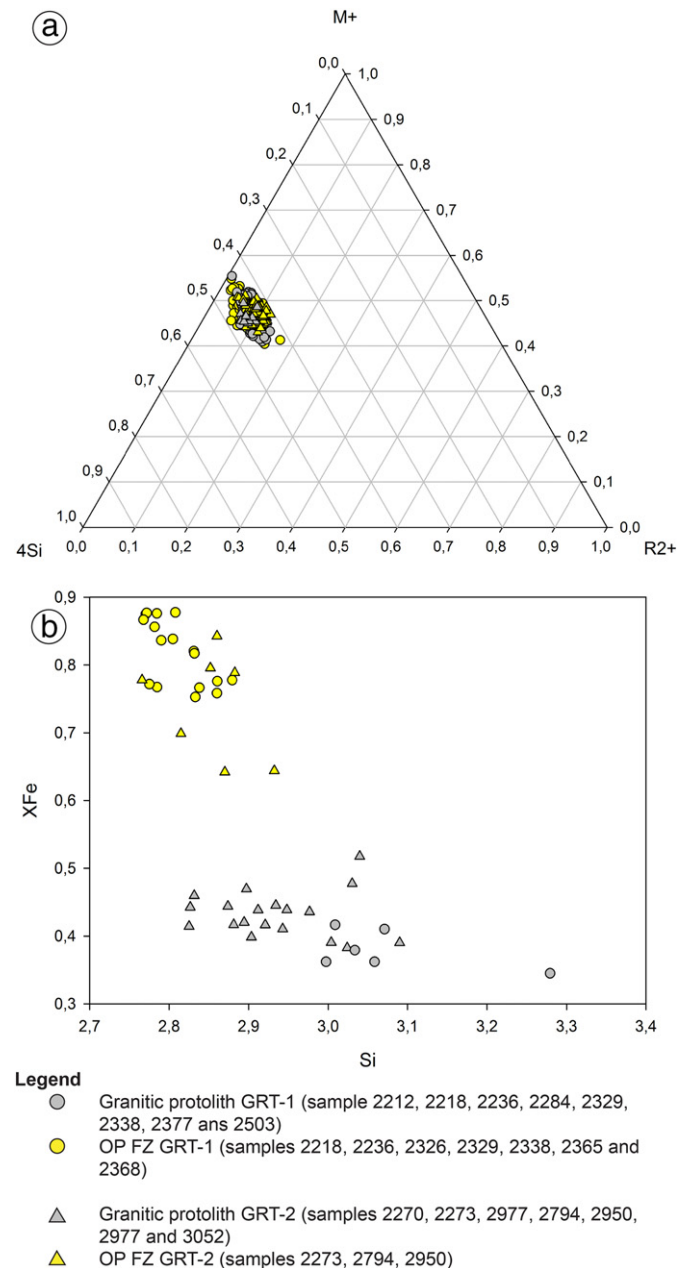
Fig. 7. Plot of the structural formulae of a) the illitic minerals in a M + -R2 + -4Si ternary diagram and b) chlorite in a diagram of XFe versus Si for wells GRT-1 and GRT-2. XFe = Fe/(Fe + Mg). The average structural formula for each sample is presented in Supplementary material 4.

zone and below (i.e. from 2329 to 2503 m MD) present an XFe ratio ≥ 0.5.

Two types of chlorite were distinguished based on their structural formulae. Samples associated to sealed fracture zone at the top of the granitic basement, at 2218 m MD, and in the main OP fracture zone, at 2368 m MD, contain Fe-rich chlorite with XFe > 0.80 (Fig. 7a). The deepest sample in GRT-1 associated to granitic protolith, at 2503 m MD, contains ferromagnesian chlorite with XFe = 0.38.

7.2. Observations in GRT-2

The chemical analyses of the illitic minerals (WCI + PCI + ml I/S) in GRT-2 do not demonstrate major variations with depth (Fig. 7b). The interlayer charge varies between 0.85 and 0.91, and the average octahedral Al content is 1.63 ± 0.07 per $O_{10}(OH)$ (Supplementary material

4). Samples in OP fracture zones, i.e. at 2270, 2773, 2950, and 3052 m MD, present an XFe ratio (~0.5) similar to that of samples associated to the granitic protolith, i.e. at 2794 and 2977 m MD.

Two types of chlorite were distinguished based on their structural formulae. Samples in OP fracture zones, i.e. at 2773, 2794 and 2950 m MD, contain Fe-rich chlorites with XFe > 0.60 (Fig. 7b). Ferromagnesian chlorite with XFe < 0.5 is observed in samples in OP fracture zones, i.e. at 2770, 2773, 2950, and 3052 m MD, as well as in the sample at 2977 MD associated to the granitic protolith (Fig. 7b).

In conclusion, the illitic minerals in both wells exhibit similar compositions regardless of the size of the illitic minerals, the occurrences of OP fracture zones or the alteration facies of the granitic basement (Fig. 7a). Chlorite occurs as two distinct populations: Fe,Mg-chlorite, which corresponds to the large sheets observed by microscopy, resulting from the alteration of biotite (Fig. 5g); and Fe-chlorite, which forms aggregates of small flakes or epitaxial growths along pore walls, formed during later hydrothermal events (Fig. 5g and b). Fe-chlorite is associated with OP fracture zones, whereas Fe,Mg-chlorite is observed regardless of the occurrence of OP fracture zones and the alteration facies of the granitic basement.

8. Discussion

8.1. Interpretation of the alteration assemblages in the granitic basement

The characterizations of the alteration petrography and of the secondary mineralogies of the cuttings collected from the two wells investigated in this study help to refine the hydrothermal history of the granitic basement at Rittershoffen (Fig. 8).

8.1.1. Early alteration stage in the poorly fractured granitic basement
Petrographic observations of the basement rocks from the parts of the wells that preserve the characteristics of strong fracture-controlled

alteration features reveal that the entire granitic batholith has been affected by an earlier alteration stage consisting of the pervasive replacement of biotite and primary calc-silicate minerals with an assemblage of Fe,Mg-chlorite, epidote and illite (Fig. 8). This type of alteration and its consequent mineral assemblage correspond to the propylitic alteration facies reported in the literature (Lowell and Guilbert, 1970). Propylitic alteration is very common in magmatic intrusive bodies. This alteration occurs during the cooling of an igneous intrusion, and results from interactions, at moderate to high temperatures (200 to 400 °C), of the most reactive igneous minerals with fluids of diverse origins that are stagnant in pores or microcracks (Reyes, 1990; Thomasson and Kristmannsdottir, 1972). Consequently, propylitic alteration can affect large volumes of intrusive rocks, and it is representative of hydrothermal alteration in inactive flow regimes (Beaufort et al., 1990).

8.1.2. Subsequent alteration stages in the highly fractured granitic basement
The OP fracture zones identified within the two boreholes during the drilling operations and from the subsequent geophysical monitoring were characterized. In the well GRT-1, OP fracture zones correlate with HEXT and HHIG facies, whereas in the well GRT-2, they correlate with HHIG and HMOD facies (Figs. 2 and 3 and Supplementary material 3). According to petrographic observations of cuttings from these facies, three different mineral assemblages can be distinguished based on the following parageneses:

- Illite + quartz + hematite ± calcite
- Illite + Fe-chlorite ± pyrite
- Illite + ml I/S + hematite ± calcite

These three parageneses crystallized under different physico-chemical conditions and reveal typical multistage hydrothermal crystallization (Fig.

Fig. 8. Paragenesis sequence and alteration history of the granitic basement at Rittershoffen.

8). The strong illitization of the wall rock in these facies could completely obliterate the features of the earlier propylitic alteration, and in some cases, strong illitization dominated by mixed layers I/S could even obliterate minerals from earlier hydrothermal parageneses (Fig. 8). For example, in HEXT facies in the well GRT-1, chlorite is no longer observed and was likely replaced completely by illite and mixed layers I/S. The relative timing of the hydrothermal events that promoted these mineral assemblages is not strictly constrained due to the absence of core samples.

It is important to note that similar mineral parageneses have been observed in the geothermal wells of Soultz (Genter, 1989; Genter and Traineau, 1992; Jacquemont, 2002; Ledésert et al., 1999), in which the occurrence of illitic minerals in fractures of core samples has been dated to more than five different geological ages from the Permian to the Eocene (Bartier et al., 2008; Clauer et al., 2008; Schleicher et al., 2006). Moreover, these clay minerals were not found at isotopic equilibrium within the currently circulating fluids at either Soultz or Rittershoffen (Table 1). Only calcite was found to be in isotopic equilibrium with the existing fluids (Fouillac and Genter, 1992). Nevertheless, the isotopic composition of the mixed layers I/S has not yet been determined because of the difficulty in separating these phases from other illitic minerals and because their relationship with the subsurface geothermal fluids is still questionable.

8.2. Illitic signature of paleo-circulation systems and OP fracture zones

Illitic minerals are known to be potential indicators of fluid circulation and paleo-circulation systems (Flexser, 1991; Harvey and Browne, 1991; Patrier et al., 1996; Teklemariam et al., 1996; Mas et al., 2003, 2006).

Observations of cuttings, macroscopically by a hand lens and microscopically in thin sections, reveal that the highest illitization occurs above 2380 m TVD in the well GRT-1 (HEXT and HHIG) and above 2470 m TVD in the well GRT-2 (HHIG and HMOD). These sections of strong illitization suggest that intense paleo-circulation systems were concentrated in the first 200 m of the granitic basement in GRT-1 and in the first 300 m of the granitic basement in GRT-2. Both sections of strong illitization are delimited at the base by main OP fracture zones in both wells.

XRD results obtained for the well GRT-1 confirm the observations of cuttings. The main OP fracture zone acts as an interface between two highly distinct sections. The uppermost section is associated with a low proportion of WCI correlated with the occurrence of mixed layers I/S that suggest intense paleo-circulations. This uppermost section correlates with HEXT and HHIG facies. The deepest section is associated with a high proportion of WCI correlated with the absence of mixed layers I/S. This deepest section correlates with HHIG, HMOD and HLOW facies.

The XRD results obtained for the well GRT-2 do not indicate two sections delimited by the main OP fracture zone, as observed for cuttings and GRT-1. XRD results reveal local variations that correlate with the three OP fracture zones in the granitic basement. The three OP fracture zones are associated with a local decrease in WCI, a local increase in PCI and occurrences of mixed layers I/S regardless of the alteration facies. These variations in the XRD results could be linked to local variations in the physico-chemical conditions in OP fracture zones. In an OP fracture zone that channels ascending geothermal fluids that are strongly oversaturated with respect to the surrounding clay minerals, abrupt changes in the flow regime, including the mixing of geothermal fluids, can lead to the explosive nucleation of small clay crystallites and promote the occurrence of heterogeneous mineral assemblages, such as mixed layers I/S (Beaufort et al., 1996; Patrier et al., 1996).
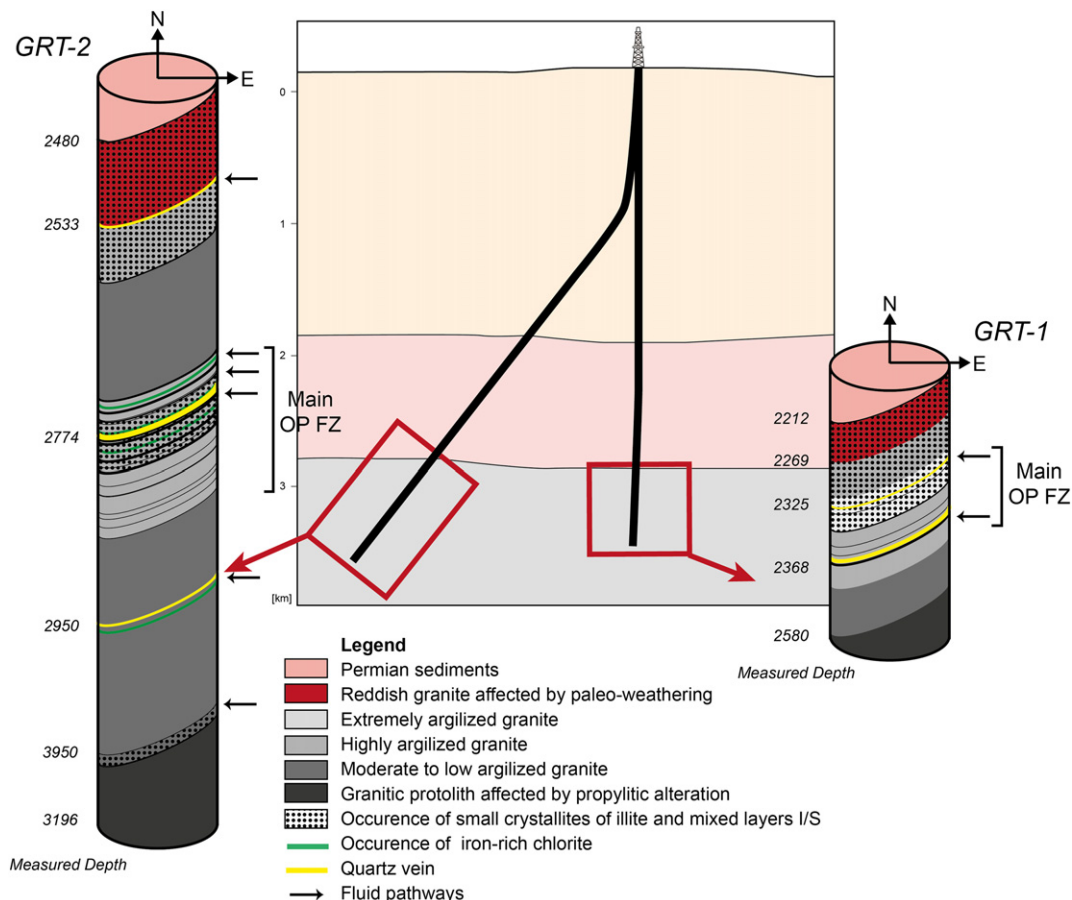

Fig. 9. Conceptual model of alteration from the clay minerals along open-holes of wells GRT-1 and GRT-2.

The chemical analyses of the illitic minerals in the Rittershoffen wells are quite consistent, and thus, we can suppose that the fluid did not evolve over time (Fig. 7a).

Even if mixed layers I/S can result from both past and present-day hydrothermal events, the occurrence of mixed layers I/S appears to be the signature of the OP fracture zones in the Rittershoffen wells (Fig. 9). Mixed layers I/S occur in the main OP fracture zone in the well GRT-1 and in three OP fracture zones in the well GRT-2. However, extensive precipitations of mixed layers I/S could lead to plugging of the OP fracture zones, thereby decreasing their natural permeability. In the well GRT-1, for example, primary and earlier secondary minerals are completely replaced by mixed layers I/S in the main OP fracture zone, and the permeability is reduced to the point that the well needs to be stimulated to bring it into production.

8.3. Chlorite signature in OP fracture zones

Two populations of chlorite were observed in the wells GRT-1 and GRT-2 (Fig. 7b). Ferromagnesian chloritic minerals associated with propylitic alteration occur throughout the granitic batholith. These minerals originate from the alteration of biotite under oxidizing conditions. It has been demonstrated that the chemistries of chloritic minerals are rock-dominated during propylitic alteration (Beaufort et al., 1992; López-Munguira et al., 2002; Mas et al., 2006) and that the incorporation of magnesium is promoted within the structure of chlorite, which crystallizes with iron oxides such as hematite under oxidizing conditions (Beaufort et al., 1992). It has also been demonstrated that the chemistry of Fe-chlorite is likely controlled by fluids circulating in the permeable fracture zones under reducing conditions (Beaufort et al., 2015; Mas et al., 2006; Patrier et al., 1996). Both of these chlorites are associated with higher temperatures than those in the present-day wells, and they do not represent current hydrothermal circulation. However, the persistence of Fe-chlorite in the OP fracture zones of GRT-2 indicates that these minerals have yet to be completely destabilized by oxidizing fluids, which are currently crystallizing mixed layers I/S (Fig. 9). The OP fracture zones of GRT-2 show higher natural permeabilities than the main OP fracture zone in GRT-1.

9. Conclusions

The alteration petrography within the granitic basement of two deep geothermal wells at Rittershoffen, GRT-1 and GRT-2, was investigated with a special focus on the clay minerals and their influence on permeability. The whole granitic basement was affected by a pervasive early stage of propylitic alteration, with the crystallization of Fe,Mg-chlorite, illite and epidote. Several stages of fluid circulation occurred later within OP fracture zones and led to subsequent alteration of the granite. These stages can be identified based on several mineral assemblages dominated by illitic minerals that formed successively. OP fracture zones in both wells are associated with occurrences of small crystallites of illite and mixed layers I/S (~10% smectite) that are the clay signatures of zones of circulation at Rittershoffen. However, the abundance of small crystallites of illite and mixed layers I/S could lead to plugging of the fracture network. When small crystallites of illite and mixed layers I/S do not completely obliterate minerals from previous hydrothermal parageneses, as observed for the well GRT-2, the natural permeability of OP fracture zones is higher and the corresponding well does not require stimulation.

Supplementary data

Supplementary data to this article can be found online at https://doi.org/10.1016/j.jvolgeores.2017.10.019.

References

Baillieux, P., Schill, E., Edel, J.-B., Mauri, G., 2013. Localization of temperature anomalies in the Upper Rhine Graben: insights from geophysics and neotectonic activity. Int. Geol. Rev. 55:1744–1762. https://doi.org/10.1080/00206814.2013.794914.

Baillieux, P., Schill, E., Abdelfettah, Y., Dezayes, C., 2014. Possible natural fluid pathways from gravity pseudo-tomography in the geothermal fields of northern Alsace (Upper Rhine Graben). Geotherm. Energy 2. https://doi.org/10.1186/s40517-014-0016-y.

Bartier, D., Ledésert, B., Clauer, N., Meunier, A., Liewig, N., Morvan, G., Addad, A., 2008. Hydrothermal alteration of the Soultz-sous-Forêts granite (hot fractured rock geothermal exchanger) into a tosudite and illite assemblage. Eur. J. Mineral. 20:131–142. https://doi.org/10.1127/0935-1221/2008/0020-1787.

Barton, C.A., Zoback, M.D., Moos, D., 1995. Fluid flow along potentially active faults in crystalline rock. Geology 23:683–686. https://doi.org/10.1130/0091-7613(1995)023<0683:FFAPAF>2.3.CO;2.

Baujard, C., Genter, A., Dalmais, E., Maurer, V., Hehn, R., Rosillette, R., Vidal, J., Schmittbuhl, J., 2017. Hydrothermal characterization of wells GRT-1 and GRT-2 in Rittershoffen, France: implications on the understanding of natural flow systems in the Rhine graben. Geothermics 65:255–268. https://doi.org/10.1016/j.geothermics.2016.11.001.

Beaufort, D., Westercamp, D., Legendre, O., Meunier, A., 1990. The fossil hydrothermal system of Saint Martin, Lesser Antilles: geology and lateral distribution of alterations. J. Volcanol. Geotherm. Res. 40:219–243. https://doi.org/10.1016/0377-0273(90)90122-V.

Beaufort, D., Patrier, P., Meunier, A., Ottaviani, M.M., 1992. Chemical variations in assemblages including epidote and/or chlorite in the fossil hydrothermal system of Saint Martin (Lesser Antilles). J. Volcanol. Geotherm. Res. 51:95–114. https://doi.org/10.1016/0377-0273(92)90062-I.

Beaufort, D., Papapanagiotou, P., Patrier Mas, P., Fouillac, A.M., Traineau, H., 1996. I/S and C/S mixed layers, some indicators of recent physical-chemical changes in active geothermal systems: The case study of Chipilapa (El Salvador). Proceedings of Seventeenth Workshop on Geothermal Reservoir Engineering. Stanford University, California, USA.

Beaufort, D., Rigault, C., Billon, S., Billault, V., Inoue, A., Inoue, S., Patrier, P., 2015. Chlorite and chloritization processes through mixed-layer mineral series in low-temperature geological systems – a review. Clay Miner. 50:497–523. https://doi.org/10.1180/claymin.2015.050.4.06.

Benderitter, Y., Tabbagh, A., Elsass, P., 1995. Calcul de l'effet thermique d'une remontée hydrothermale dans le socle fracturé. Application à l'anomalie géothermique de Soultz-sous-Forêts (Nord Alsace). Bull. Soc. Geol. Fr. 1, 37–48.

Bradford, J., McLennan, J., Moore, J., Glasby, D., Waters, D., Kruwells, R., Bailey, A., Rickard, W., Bloomfield, K., King, D., 2013. Recent developments at the Raft River geothermal field. Proceedings of Thirty-Eighth Workshop on Geothermal Reservoir Engineering. Stanford University, California, USA.

Brindley, G.W., Brown, G., 1980. X-ray Diffraction procedures for clay mineral identification. In: Brindley, G.W., Brown, G. (Eds.), Crystal Structures of Clay Minerals and Their X-Ray Identification, pp. 305–360 London, Great Britain.

Browne, P.R.L., Ellis, A.J., 1970. The Ohaki-Broadlands hydrothermal area, New Zealand; mineralogy and related geochemistry. Am. J. Sci. 269:97–131. https://doi.org/10.2475/ajs.269.2.97.

Clauer, N., Liewig, N., Ledesert, B., Zwingmann, H., 2008. Thermal history of Triassic sandstones from the Vosges Mountains-Rhine Graben rifting area, NE France, based on K-Ar illite dating. Clay Miner. 43:363–379. https://doi.org/10.1180/claymin.2008.043.3.03.

Davatzes, N.C., Hickman, S.H., 2005. Controls on fault-hosted fluid flow; Preliminary results from the Coso Geothermal Field, CA. In: Geothermal Resources Council Transactions (Ed.), Geothermal Resources Council. Davis, California, pp. 343–348.

Flexser, S., 1991. Hydrothermal alteration and past and present thermal regimes in the western moat of Long Valley caldera. J. Volcanol. Geotherm. Res. 48:303–318. https://doi.org/10.1016/0377-0273(91)90048-5.

Fouillac, A.M., Genter, A., 1992. An O, D, C isotopic study of water/rock interactions in the sSoultz-sous-Forêts granite. Drillhole GPK-1, HDR Site, Alsace. In: Bresee, James C.

(Ed.), Geothermal Energy in Europe - The Soultz Hot Dry Rock Project, pp. 105–117 Montreux, Switzerland.

Genter, A., 1989. Géothermie roches chaudes sèches: le granite de Soultz-sous-Forêts (Bas-Rhin, France). Fracturation naturelle, altérations hydrothermales et interaction eau-roche. (PhD thesis). Université d'Orléans, France.

Genter, A., Traineau, H., 1992. Hydrothermally altered and fractured granite as an HDR reservoir in the EPS-1 borehole, Alsace, France. Proceedings of Seventeenth Workshop on Geothermal Reservoir Engineering. Stanford University, California, USA.

Genter, A., Evans, K., Cuenot, N., Fritsch, D., Sanjuan, B., 2010. Contribution of the exploration of deep crystalline fractured reservoir of Soultz to the knowledge of enhanced geothermal systems (EGS). Compt. Rendus Geosci. 342:502–516. https://doi.org/10.1016/j.crte.2010.01.006.

Geoportail of EU-Project GeORG - INTERREG IV Upper Rhine. [WWW Document]. http://www.geopotenziale.org, Accessed date: 14 April 2016.

Harvey, C.C., Browne, P.R.L., 1991. Mixed-layer clay geothermometry in the Wairakei geothermal field, New Zealand. Clay Clay Miner. 39:614–621. https://doi.org/10.1346/ccmn.1991.0390607.

Hooijkaas, G.R., Genter, A., Dezayes, C., 2006. Deep-seated geology of the granite intrusions at the Soultz EGS site based on data from 5 km-deep boreholes. Geothermics 35:484–506. https://doi.org/10.1016/j.geothermics.2006.03.003.

Jacquemont, B., 2002. Etude des intéractions eaux-roches dans le granite de Soultz-sous-Forêts; Quantification et modélisation des transferts de matière par les fluides. (PhD thesis). Université de Strasbourg, France.

Kubler, B., 1968. Evaluation quantitative du métamorphisme par la cristallinité de l'illite: Etat des progrès réalisés ces dernières années. Bull. Cent. Rech. Pau-SNPA 2, 385–397.

Lanson, B., Beaufort, D., Berger, G., Petit, S., Lacharpagne, J.-C., 1995. Evolution of clay minerals crystallographic structure in the dutch Rotliengende sandstone reservoir. Bull. Centres Rech. Explor. Prod. Elf-Aquitaine 19, 243–265.

Ledésert, B., Berger, G., Meunier, A., Genter, A., Bouchet, A., 1999. Diagenetic-type reactions related to hydrothermal alteration in the Soultz-sous-Forêts Granite, France. Eur. J. Mineral. 11:731–741. https://doi.org/10.1127/ejm/11/4/0731.

López-Munguira, A., Nieto, F., Morata, D., 2002. Chlorite composition and geothermometry: a comparative HRTEM/AEM-EMPA-XRD study of Cambrian basic lavas from the Ossa Morena Zone, SW Spain. Clay Clay Miner. 37:267–281. https://doi.org/10.1180/0009855023720033.

Lowell, J.D., Guilbert, J.M., 1970. Lateral and vertical alteration-mineralization zoning in porphyry ore deposits. Econ. Geol. 65:373–408. https://doi.org/10.2113/gsecongeo.65.4.373.

Mas, A., Patrier, P., Beaufort, D., Genter, A., 2003. Clay-mineral signatures of fossil and active hydrothermal circulations in the geothermal system of the Lamentin Plain, Martinique. J. Volcanol. Geotherm. Res. 124:195–218. https://doi.org/10.1016/S0377-0273(03)00044-1.

Mas, A., Guisseau, D., Patrier Mas, P., Beaufort, D., Genter, A., Sanjuan, B., Girard, J.P., 2006. Clay minerals related to the hydrothermal activity of the Bouillante geothermal field (Guadeloupe). J. Volcanol. Geotherm. Res. 158:380–400. https://doi.org/10.1016/j.jvolgeores.2006.07.010.

Patrier, P., Papapanagiotou, P., Beaufort, D., Traineau, H., Bril, H., Rojas, J., 1996. Role of permeability versus temperature in the distribution of the fine (<0.2 μm) clay fraction in the Chipilapa geothermal system (El Salvador, Central America). J. Volcanol. Geotherm. Res. 72:101–120. https://doi.org/10.1016/0377-0273(95)00078-X.

Pribnow, D., Clauser, C., 2000. Heat and fluid flow at the Soultz Hot Dry Rock system in the Rhine Graben. Proceedings of World Geothermal Congress 2000. Kyushu - Tohoku, Japan.

Pribnow, D., Schellschmidt, R., 2000. Thermal tracking of upper crustal fluid flow in the Rhine graben. Geophys. Res. Lett. 27.

Reyes, A.G., 1990. Petrology of Philippine geothermal systems and the application of alteration mineralogy to their assessment. J. Volcanol. Geotherm. Res. 43:279–309. https://doi.org/10.1016/0377-0273(90)90057-M.

Sanjuan, B., Millot, R., Dezayes, C., Brach, M., 2010. Main characteristics of the deep geothermal brine (5 km) at Soultz-sous-Forêts (France) determined using geochemical and tracer test data. Compt. Rendus Geosci. 342:546–559. https://doi.org/10.1016/j.crte.2009.10.009.

Sanjuan, B., Millot, R., Ásmundsson, R., Brach, M., Giroud, N., 2014. Use of two new Na/Li geothermometric relationships for geothermal fluids in volcanic environments. Chem. Geol. 389:60–81. https://doi.org/10.1016/j.chemgeo.2014.09.011.

Sanjuan, B., Millot, R., Innocent, C., Dezayes, C., Scheiber, J., Brach, M., 2016. Major geochemical characteristics of geothermal brines from the Upper Rhine Graben granitic basement with constraints on temperature and circulation. Chem. Geol. 428:27–47. https://doi.org/10.1016/j.chemgeo.2016.02.021.

Schellschmidt, R., Clauser, C., 1996. The thermal regime of the Upper Rhine Graben and the anomaly at Soultz. Z. Für Angew. Geol. 42, 40–44.

Schleicher, A.M., Warr, L.N., Kober, B., Laverret, E., Clauer, N., 2006. Episodic mineralization of hydrothermal illite in the Soultz-sous-Forêts granite (Upper Rhine Graben, France). Contrib. Mineral. Petrol. 152:349–364. https://doi.org/10.1007/s00410-006-0110-7.

Teklemariam, M., Battaglia, S., Gianelli, G., Ruggieri, G., 1996. Hydrothermal alteration in the Aluto-Langano geothermal field, Ethiopia. Geothermics 25:679–702. https://doi.org/10.1016/S0375-6505(96)00019-3.

Thomasson, J., Kristmannsdottir, H., 1972. High temperature alteration minerals and thermal brines, Reykjanes, Iceland. Contrib. Mineral. Petrol. 36:123–134. https://doi.org/10.1007/bf00371183.

Traineau, H., Genter, A., Cautru, J.-P., Fabriol, H., Chèvremont, P., 1992. Petrography of the granite massif from drill cutting analysis and well log interpretation in the geothermal HDR borehole GPK-1 (Soultz, Alsace, France). In: Bresee, James C. (Ed.), Geothermal Energy in Europe - The Soultz Hot Dry Rock Project, pp. 1–29 Montreux, Switzerland.

Vidal, J., Genter, A., Schmittbuhl, J., 2016a. Pre- and post-stimulation characterization of geothermal well GRT-1, Rittershoffen, France: insights from acoustic image logs of hard fractured rock. Geophys. J. Int. 206:845–860. https://doi.org/10.1093/gji/ggw181.

Vidal, J., Ulrich, M., Whitechurch, H., Genter, A., Schmittbuhl, J., Dalmais, E., Girard-Berthet, V., 2016b. Hydrothermal Alteration of the Hidden Granite in the Geothermal Context of the Upper Rhine Graben. Proceedings of Forty-First Workshop on Geothermal Reservoir Engineering. Stanford University, California, USA.

Vidal, J., Genter, A., Chopin, F., 2017. Permeable fracture zones in the hard rocks of the geothermal reservoir at Rittershoffen, France. J. Geophys. Res. Solid Earth 122. https://doi.org/10.1002/2017JB014331.

Supplementary material 1 for

Clay minerals related to the circulation of geothermal fluids in boreholes at Rittershoffen (Alsace, France)

Jeanne VIDAL[1], Patricia PATRIER[2], Albert GENTER[3], Daniel BEAUFORT[2], Chrystel DEZAYES[4], Carole GLAAS[3], Catherine LEROUGE[4], Bernard SANJUAN[4]

[1] University of Strasbourg, CNRS UMR 7516 IPGS, 1 rue Blessig, F-67084 Strasbourg Cedex
[2] University of Poitiers, CNRS UMR 7285 IC2MP, HydrASA, Bat B8, Rue Albert Turpain, F-86022 Poitiers Cedex
[3] ES-Géothermie, 5 rue Lisbonne, 67300 Schiltigheim, France
[4] BRGM - 3, Av. Claude Guillemin / BP6009 - 45060 Orléans Cedex 02, France

Introduction

This supplementary material provides microscopic observations of cutting samples in the granitic basement of the well GRT-1.

Caption

1: Cutting samples in the granitic basement at 2536 m MD (GRAN_OX)

2: Cutting samples in the granitic basement at 2503 m MD (HLOW)

3: Cutting samples in the granitic basement at 2407 m MD (HMOD)

4: Cutting samples in the granitic basement at 2407 m MD (HMOD)

5: Cutting samples in the granitic basement at 2377 m MD (HHIG)

6: Cutting samples in the granitic basement at 2371 m MD (HHIG)

7: Cutting samples into the main OP fracture zone in the granitic basement at 2368 m MD (HHIG)

8: Cutting samples into the main OP fracture zone in the granitic basement at 2368 m MD (HHIG)

9: Cutting samples into the main OP fracture zone in the granitic basement at 2368 m MD (HHIG)

10: Cutting samples into the main OP fracture zone in the granitic basement at 2368 m MD (HHIG)

11: Cutting samples into the main OP fracture zone in the granitic basement at 2368 m MD (HHIG)

12: Cutting samples into the main OP fracture zone in the granitic basement at 2347 m MD (HEXT)

13: Cutting samples into the main OP fracture zone in the granitic basement at 2338 m MD (HEXT)

14: Cutting samples into the main OP fracture zone in the granitic basement at 2326 m MD (HEXT)

15: Cutting samples into the main OP fracture zone in the granitic basement at 2326 m MD (HEXT)

16: Cutting samples in the granitic basement at 2284 m MD (HHIG)

17: Cutting samples in the granitic basement at 2284 m MD (HHIG)

18: Cutting samples in the granitic basement at 2284 m MD (HHIG)

19: Cutting samples in the granitic basement at 2284 m MD (HHIG)

20: Cutting samples in the paleo-altered granitic basement at 2218 m MD (RED)

21: Cutting samples in the paleo-altered granitic basement at 2212 m MD (RED)
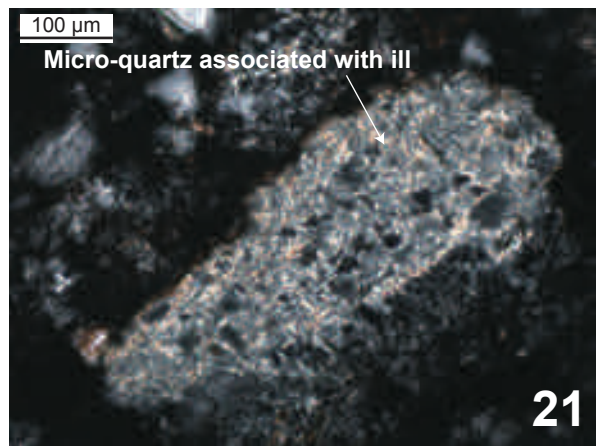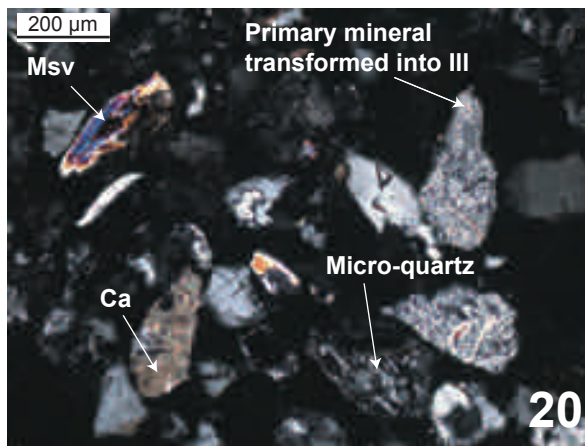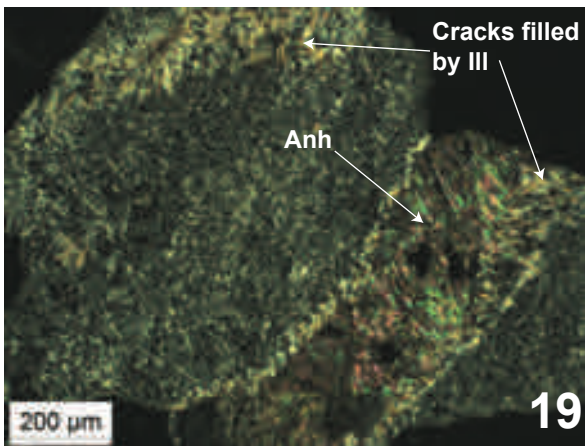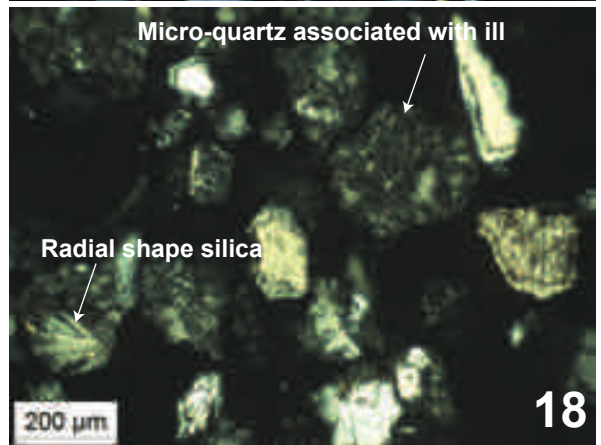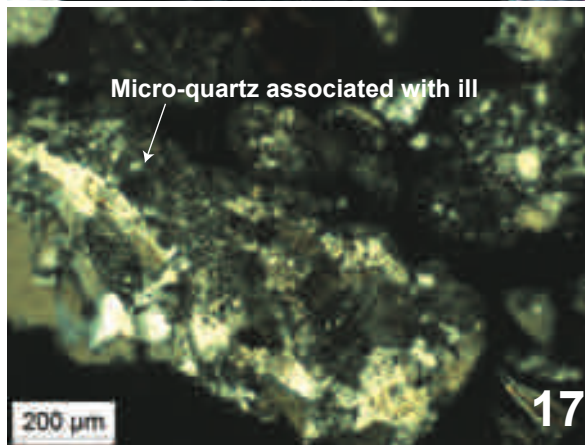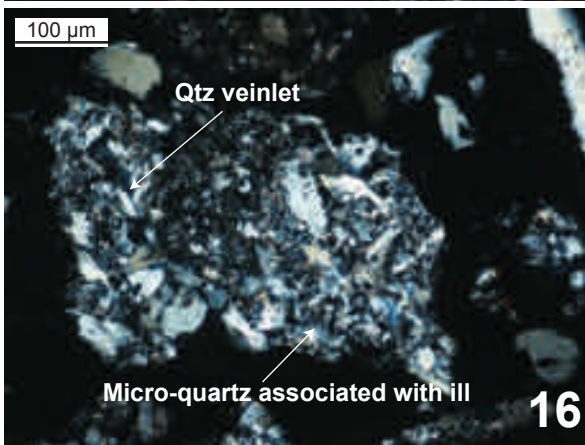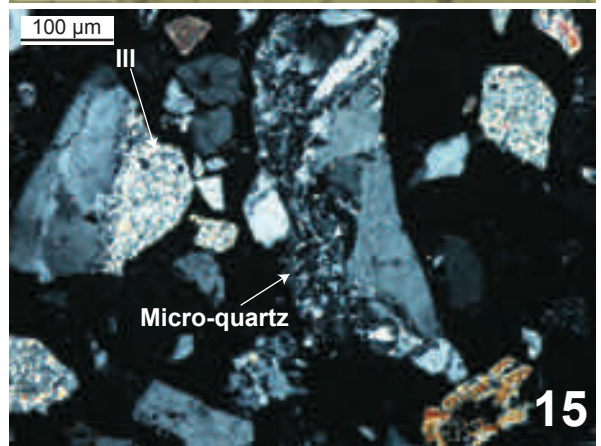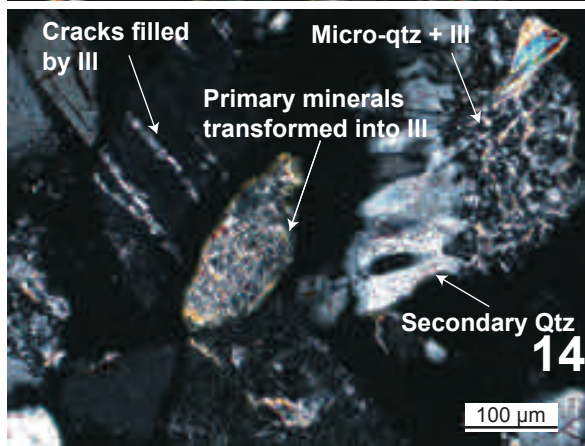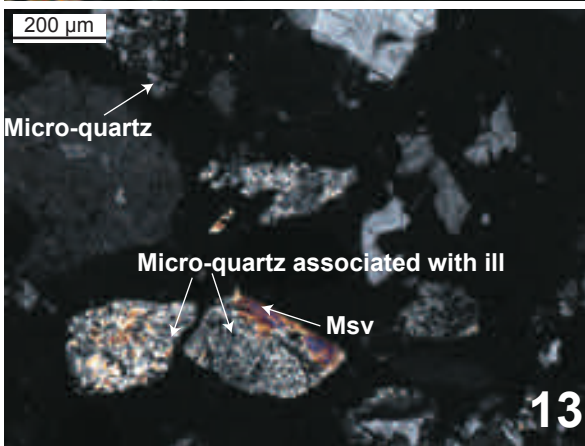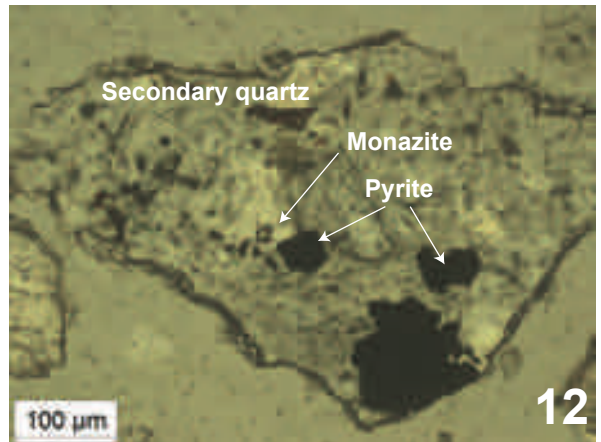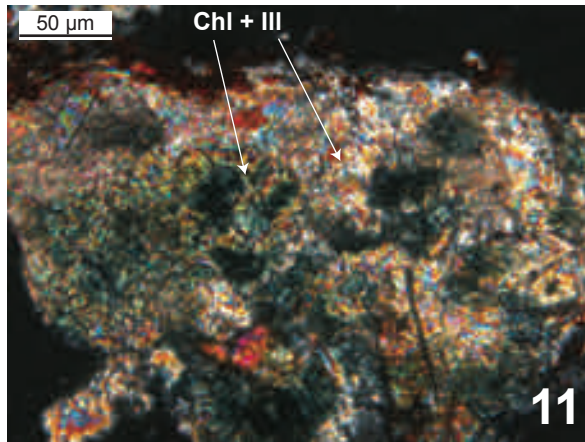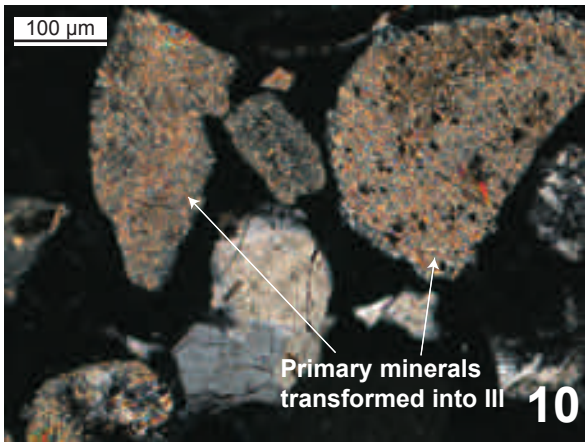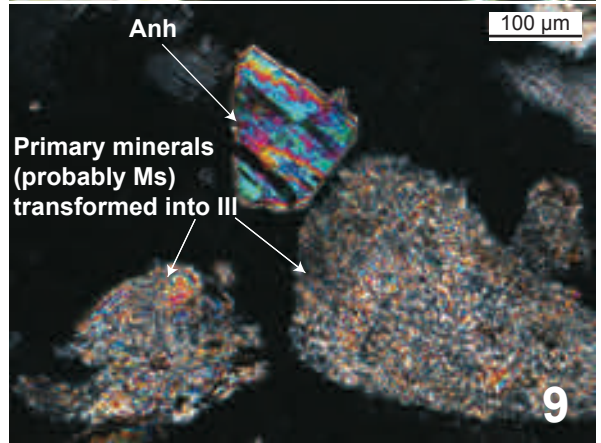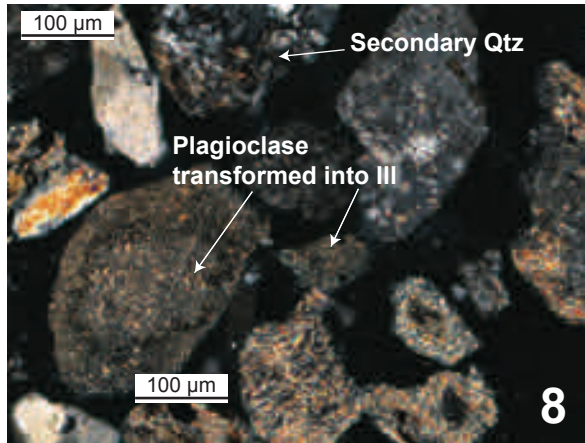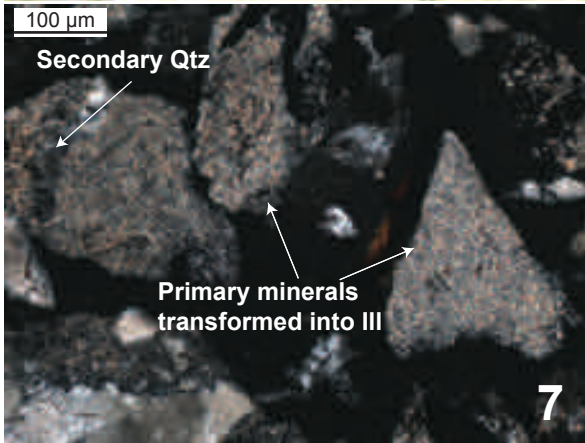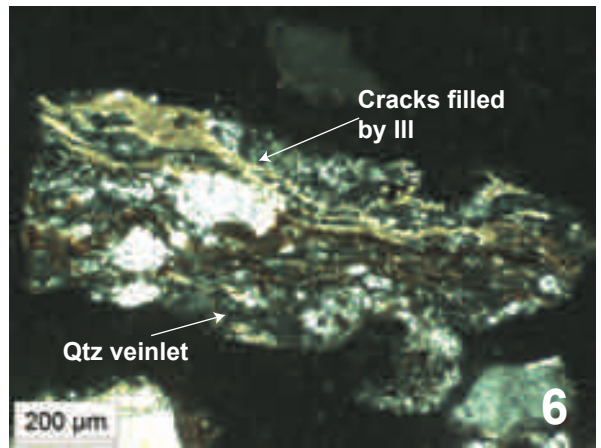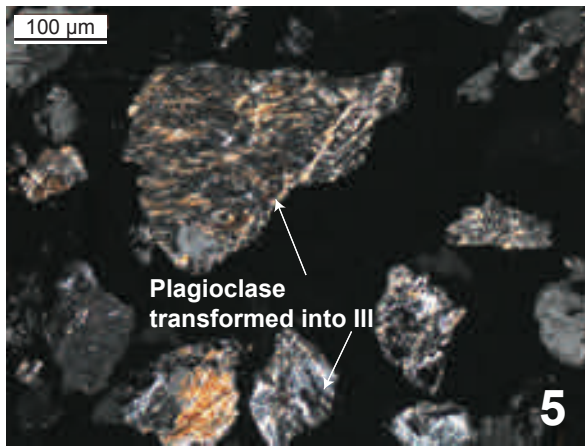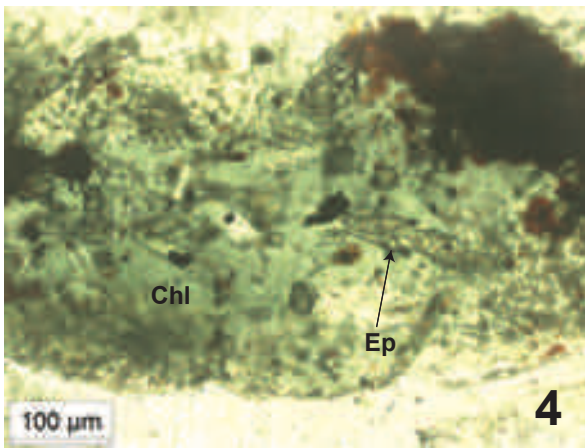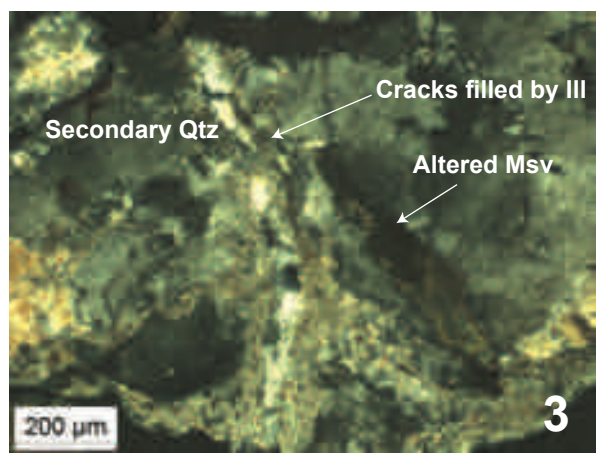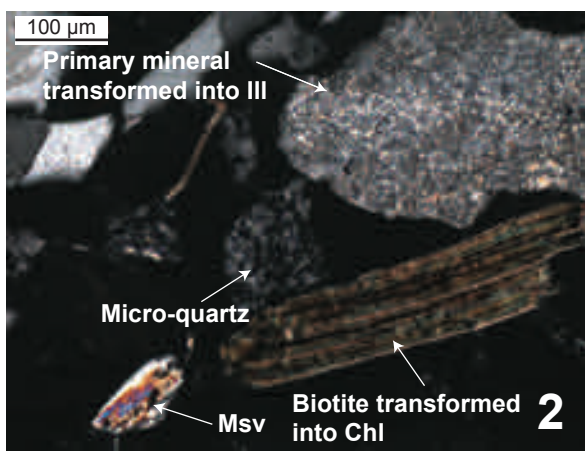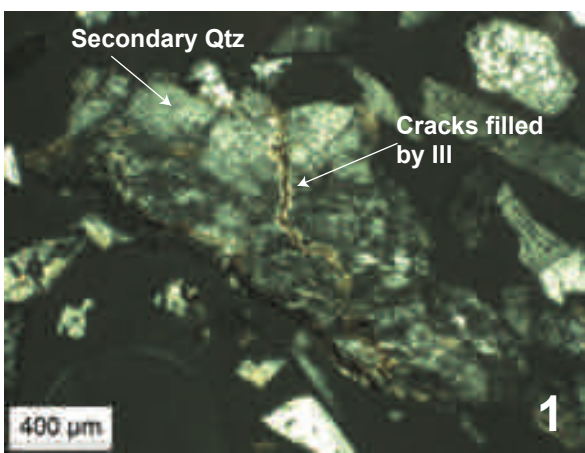
Supplementary material 2 for

Clay minerals related to the circulation of geothermal fluids in boreholes at Rittershoffen (Alsace, France)

Jeanne VIDAL[1], Patricia PATRIER[2], Albert GENTER[3], Daniel BEAUFORT[2], Chrystel DEZAYES[4], Carole GLAAS[3], Catherine LEROUGE[4], Bernard SANJUAN[4]

[1] University of Strasbourg, CNRS UMR 7516 IPGS, 1 rue Blessig, F-67084 Strasbourg Cedex
[2] University of Poitiers, CNRS UMR 7285 IC2MP, HydrASA, Bat B8, Rue Albert Turpain, F-86022 Poitiers Cedex
[3] ES-Géothermie, 5 rue Lisbonne, 67300 Schiltigheim, France
[4] BRGM - 3, Av. Claude Guillemin / BP6009 - 45060 Orléans Cedex 02, France

Introduction

This supplementary material provides microscopic observations of cutting samples in the granitic basement of the well GRT-2.

Caption

1: Cutting samples into the deep OP fracture zone in the granitic basement at 3052 m MD (HMOD)

2: Cutting samples into the deep OP fracture zone in the granitic basement at 3052 m MD (HMOD)

3: Cutting samples in the granitic basement at 2977 m MD (HLOW)

4: Cutting samples into the deep OP fracture zone in the granitic basement at 2950 m MD (HMOD)

5: Cutting samples into the main OP fracture zone in the granitic basement at 2794 m MD (HHIG)

8: Cutting samples into the main OP fracture zone in the granitic basement at 2773 m MD (HHIG)

9: Cutting samples into the main OP fracture zone in the granitic basement at 2773 m MD (HHIG)

10: Cutting samples into the main OP fracture zone in the granitic basement at 2773 m MD (HHIG)

11: Cutting samples into the main OP fracture zone in the granitic basement at 2368 m MD (HHIG)

12: Cutting samples into the main OP fracture zone in the granitic basement at 2770 m MD (HHIG)
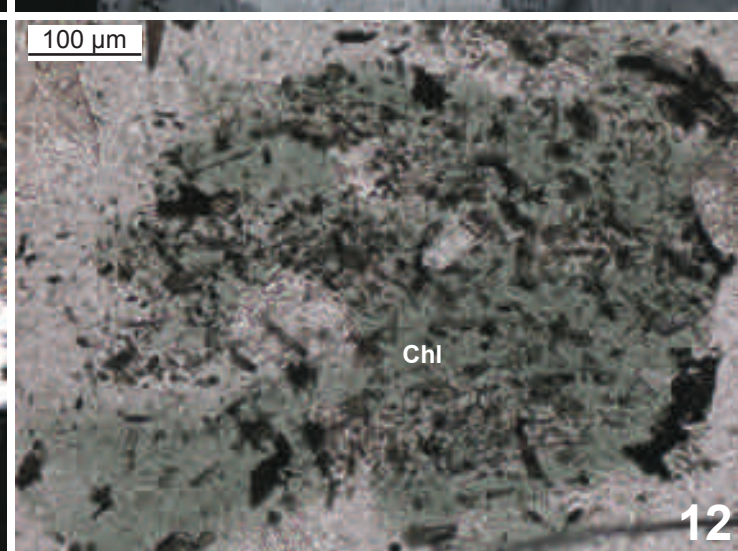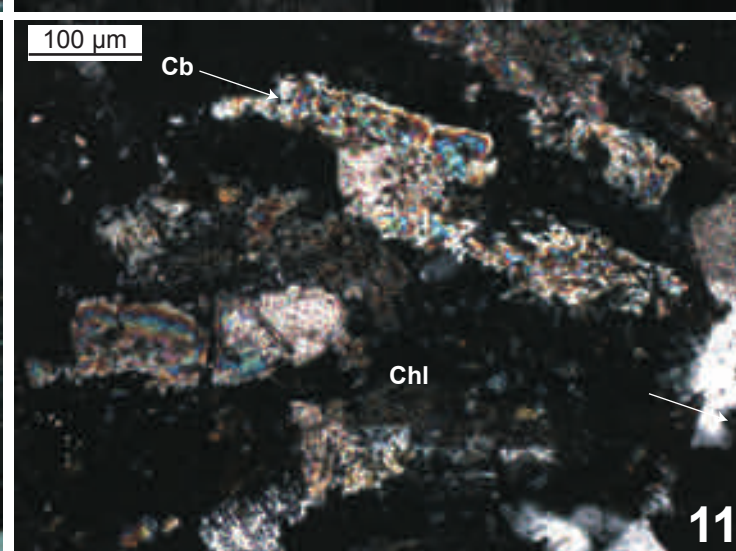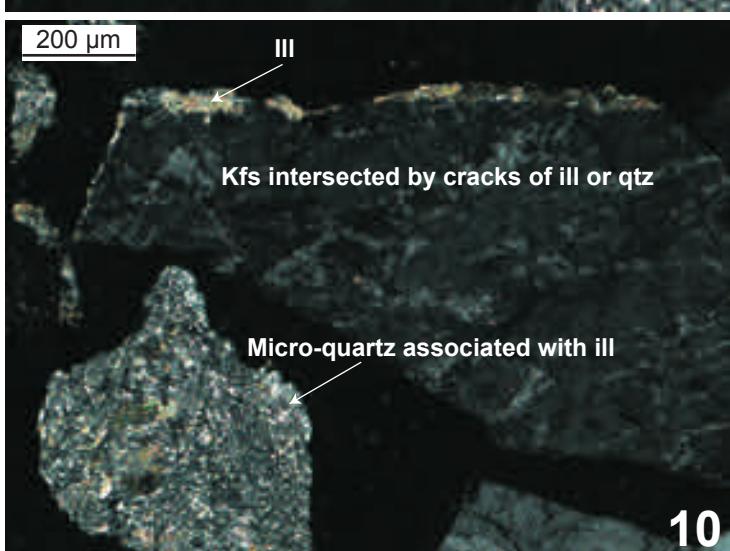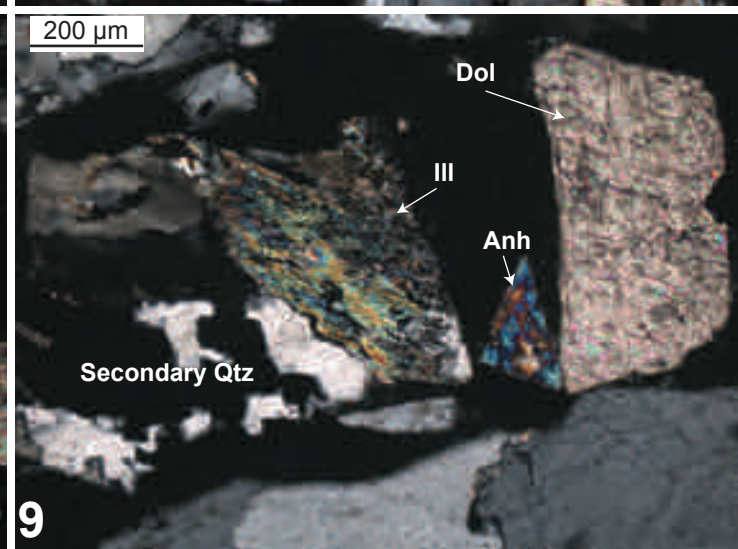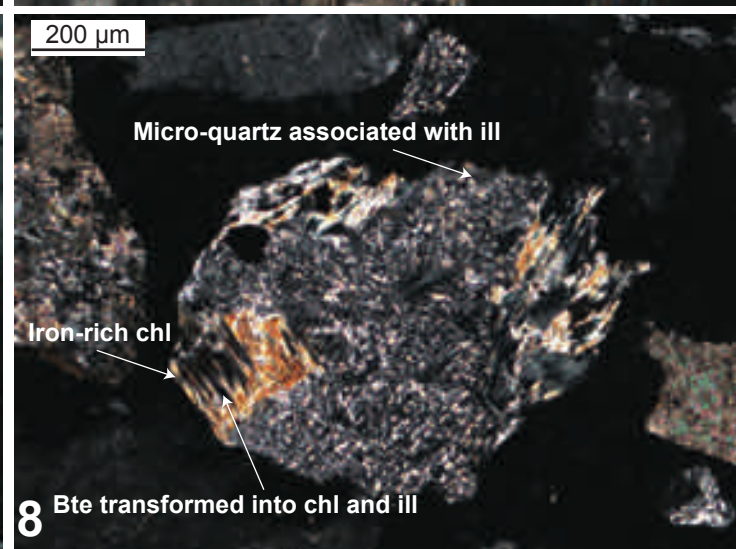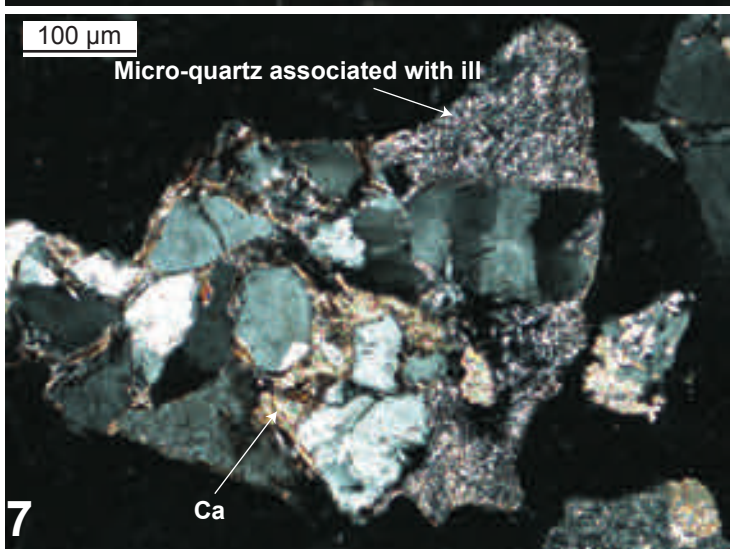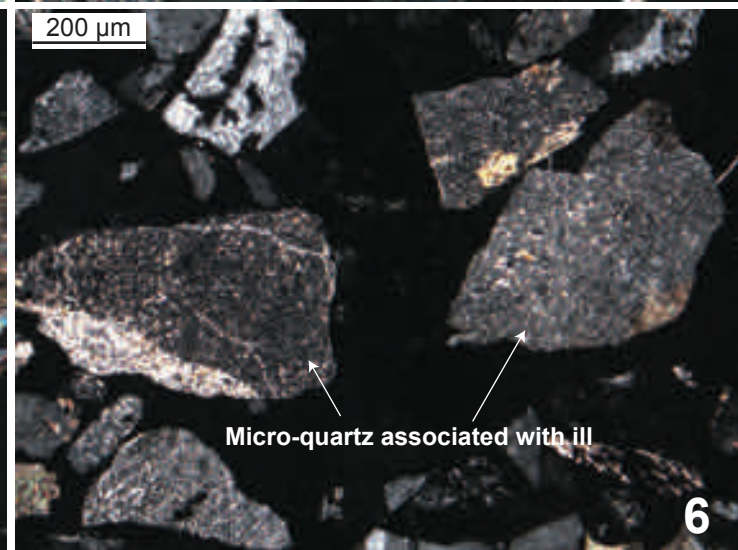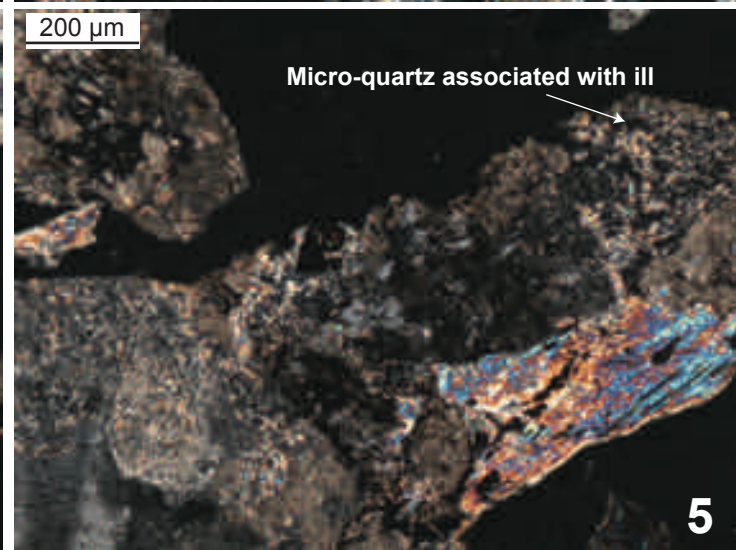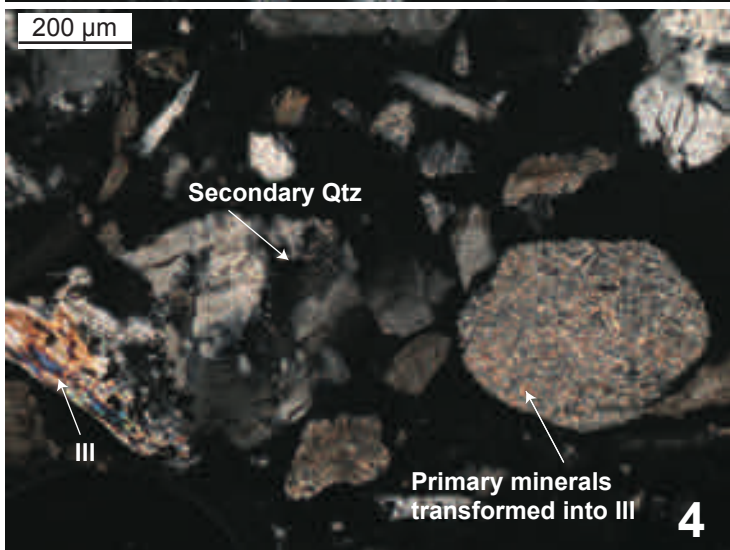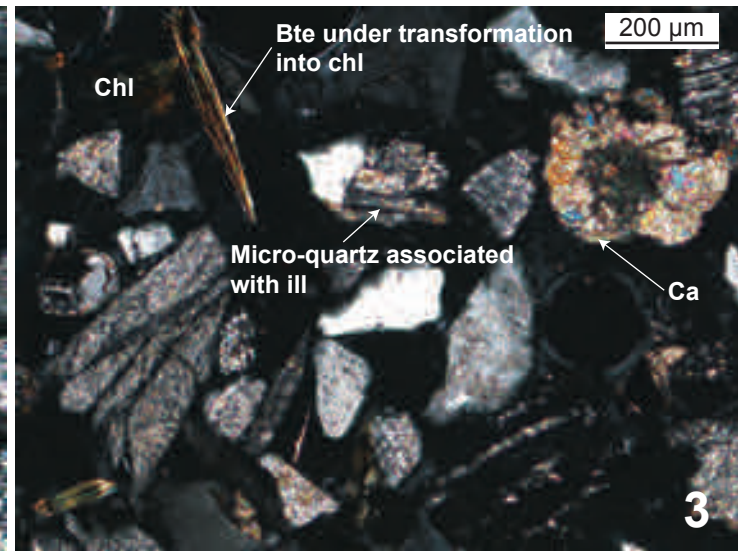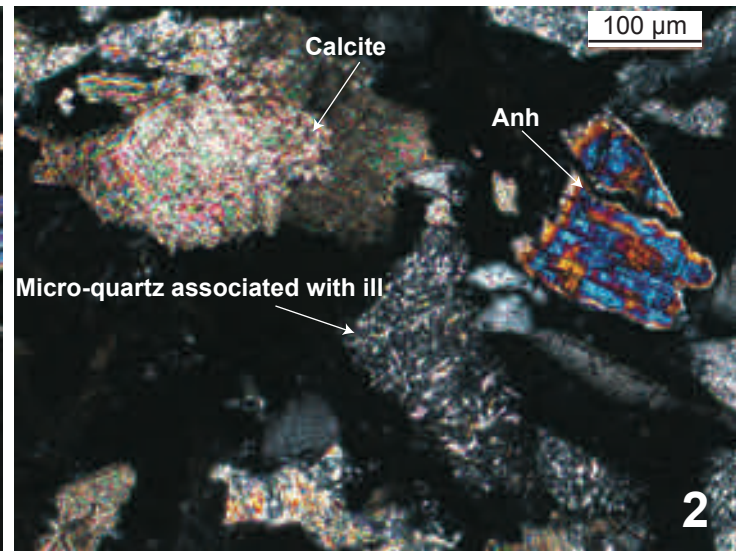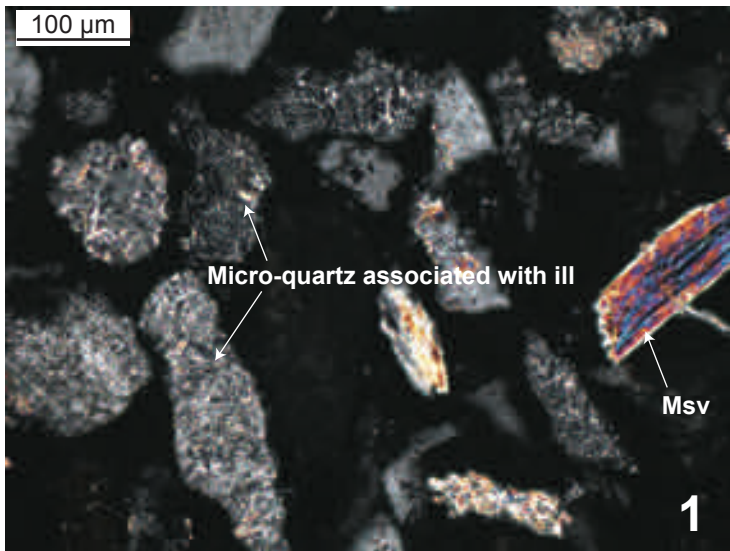
Supplementary material 3 for

Clay minerals related to the circulation of geothermal fluids in boreholes at Rittershoffen (Alsace, France)

Jeanne VIDAL[1], Patricia PATRIER[2], Albert GENTER[3], Daniel BEAUFORT[2], Chrystel DEZAYES[4], Carole GLAAS[3], Catherine LEROUGE[4], Bernard SANJUAN[4]

[1] University of Strasbourg, CNRS UMR 7516 IPGS, 1 rue Blessig, F-67084 Strasbourg Cedex
[2] University of Poitiers, CNRS UMR 7285 IC2MP, HydrASA, Bat B8, Rue Albert Turpain, F-86022 Poitiers Cedex
[3] ES-Géothermie, 5 rue Lisbonne, 67300 Schiltigheim, France
[4] BRGM - 3, Av. Claude Guillemin / BP6009 - 45060 Orléans Cedex 02, France

Introduction

This supplementary material provides a geometrical representation of degrees of alteration in the granitic basement in the wells GRT-1 and GRT-2.

Degrees of alteration are based on argilization of cuttings described in section 5 of the article. Limits of each facies intersected by wells are detailed in the table below.

Figure
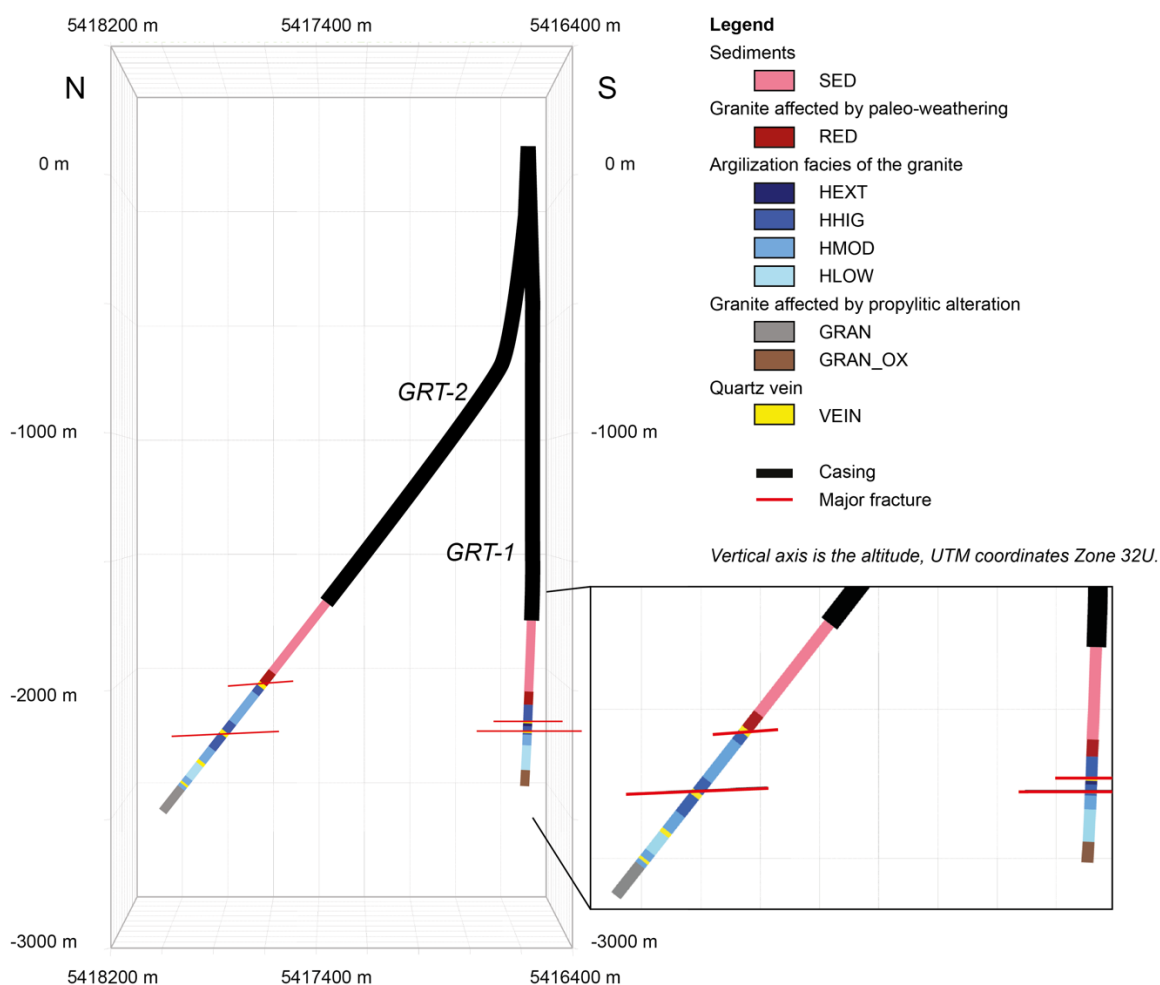
Caption

N-S cross section through the wells GRT-1 and GRT-2 (from MOVE 3D geometrical modeling) with the degrees of alteration indicated along the open-hole sections. A magnification of the open-holes is presented. Red lines are major fractures that act as fluid pathways in the main OP fracture zones of both wells. They were identified from acoustic image logs reported by Vidal et al. (2017).

RED: reddish granite
GRAN: granitic protolith
HLOW: low degree of argilization
HMOD: moderate degree of argilization
HHIG: high degree of argilization
HEXT: extreme degree of argilization

Table Facies of alteration encountered in wells GRT-1 and GRT-2 from the top to the deepest granitic basement. The top of the granitic basement is located at 2212 m MD (i.e., 2198 m TVD) in GRT-1 and at 2480 m MD (i.e., 2156 m TVD) in GRT-2.

Facies intersected by wells from the shallowest to the deepest	GRT-1			GRT-2		
	Name of the facies	Measured depth (m)	True vertical depth (m)	Name of the facies	Measured depth (m)	True vertical depth (m)
Facies 1	RED	2270	2057	RED	2533	2204
Facies 2	HHIG	2326	2310	VEIN	2536	2206
Facies 3	VEIN	2329	2314	HHIG	2578	2239
Facies 4	HEXT	2350	2334	HMOD	2737	2363
Facies 5	HHIG	2365	2349	HHIG	2770	2390
Facies 6	VEIN	2368	2352	VEIN	2791	2407
Facies 7	HHIG	2380	2364	HHIG	2875	2470
Facies 8	HMOD	2410	2393	HMOD	2944	2523
Facies 9	HLOW	2516	2498	VEIN	2950	2528
Facies 10	GRAN_OX	2580	2562	HLOW	3020	2579
Facies 11				HMOD	3046	2600
Facies 12				VEIN	3061	2610
Facies 13				GRAN	3196	2708

Supplementary material 4 for

Clay minerals related to the circulation of geothermal fluids in boreholes at Rittershoffen (Alsace, France)

Jeanne VIDAL[1], Patricia PATRIER[2], Albert GENTER[3], Daniel BEAUFORT[2], Chrystel DEZAYES[4], Carole GLAAS[3], Catherine LEROUGE[4], Bernard SANJUAN[4]

[1] University of Strasbourg, CNRS UMR 7516 IPGS, 1 rue Blessig, F-67084 Strasbourg Cedex
[2] University of Poitiers, CNRS UMR 7285 IC2MP, HydrASA, Bat B8, Rue Albert Turpain, F-86022 Poitiers Cedex
[3] ES-Géothermie, 5 rue Lisbonne, 67300 Schiltigheim, France
[4] BRGM - 3, Av. Claude Guillemin / BP6009 - 45060 Orléans Cedex 02, France

Introduction

This supplementary material provides detailed calculations of structural formulae of illitic minerals (Tables 1 and 2) and chlorite (Table 3). Results are represented in Figure 7 of the article.

Table 1 Calculations of structural formulae of some illitic minerals at various depths in GRT-1 well. n.a.: number of analyses; An. Av.: analytical average; s.d.: standard deviation; OCT: octahedral occupancy; INTCH: interlayer charge; XFe: Fe/(Fe+Mg).

Samples	GRT-1 2212		GRT-1 2218		GRT-1 2236		GRT-1 2284		GRT-1 2326		GRT-1 2329	
n. a.	13		18		15		14		29		22	
	An. Av.	s.d.	An. Av.	s.d.	An. Av.	s.d.	An. Av.	s.d.	An. Av.	s.d.	An. Av.	s.d.
Si	3,35	*0,25*	3,28	*0,20*	3,36	*0,02*	3,40	*0,04*	3,31	*0,19*	3,38	*0,12*
Al IV	0,65	*0,25*	0,72	*0,20*	0,64	*0,02*	0,60	*0,04*	0,69	*0,19*	0,62	*0,12*
Al VI	1,66	*0,18*	1,73	*0,11*	1,61	*0,13*	1,63	*0,06*	1,71	*0,21*	1,66	*0,07*
Fe 3+	0,13	*0,08*	0,11	*0,03*	0,18	*0,09*	0,16	*0,04*	0,13	*0,07*	0,14	*0,00*
Mg	0,21	*0,10*	0,16	*0,06*	0,19	*0,02*	0,19	*0,04*	0,15	*0,14*	0,18	*0,06*
Ti	0,01	*0,01*	0,01	*0,01*	0,00	*0,00*	0,00	*0,00*	0,00	*0,00*	0,00	*0,00*
Mn	0,00	*0,00*	0,00	*0,00*	0,00	*0,00*	0,00	*0,00*	0,00	*0,00*	0,00	*0,00*
OCT	2,00	*0,02*	2,01	*0,03*	1,99	*0,01*	1,98	*0,02*	1,99	*0,00*	1,99	*0,02*
Ca	0,01	*0,00*	0,01	*0,02*	0,00	*0,00*	0,00	*0,00*	0,00	*0,00*	0,00	*0,00*
Na	0,00	*0,01*	0,00	*0,01*	0,00	*0,00*	0,00	*0,00*	0,00	*0,00*	0,00	*0,00*
K	0,83	*0,08*	0,84	*0,04*	0,86	*0,04*	0,85	*0,03*	0,86	*0,06*	0,82	*0,01*
INTCH	0,85	*0,08*	0,85	*0,05*	0,87	*0,04*	0,85	*0,03*	0,86	*0,06*	0,83	*0,01*
XFe	0,38	*0,44*	0,41	*0,33*	0,49	*0,33*	0,46	*0,50*	0,46	*0,33*	0,44	*0,00*

Samples	GRT-1 2338		GRT-1 2365		GRT-1 2368		GRT-1 2377		GRT-1 2503	
n. a.	21		46		52		19		22	
	An. Av.	s.d.	An. Av.	s.d.	An. Av.	s.d.	An. Av.	s.d.	An. Av.	s.d.
Si	3,44	*0,29*	3,30	*0,06*	3,34	*0,12*	3,31	*0,08*	3,33	*0,06*
Al IV	0,56	*0,29*	0,70	*0,06*	0,66	*0,12*	0,69	*0,08*	0,67	*0,06*
Al VI	1,67	*0,07*	1,68	*0,04*	1,65	*0,09*	1,72	*0,07*	1,74	*0,06*
Fe 3+	0,14	*0,06*	0,16	*0,04*	0,17	*0,05*	0,14	*0,03*	0,11	*0,04*
Mg	0,14	*0,04*	0,14	*0,01*	0,16	*0,05*	0,12	*0,04*	0,11	*0,05*
Ti	0,00	*0,00*	0,00	*0,00*	0,00	*0,00*	0,00	*0,00*	0,00	*0,00*
Mn	0,00	*0,00*	0,00	*0,00*	0,00	*0,00*	0,00	*0,00*	0,00	*0,00*
OCT	1,95	*0,11*	1,98	*0,02*	1,98	*0,05*	1,99	*0,01*	1,96	*0,02*
Ca	0,00	*0,00*	0,00	*0,00*	0,01	*0,03*	0,00	*0,00*	0,04	*0,04*
Na	0,00	*0,00*	0,00	*0,02*	0,00	*0,00*	0,00	*0,00*	0,00	*0,00*
K	0,84	*0,14*	0,89	*0,05*	0,86	*0,05*	0,85	*0,05*	0,86	*0,04*
INTCH	0,84	*0,14*	0,90	*0,02*	0,87	*0,05*	0,85	*0,04*	0,90	*0,07*
XFe	0,50	*0,60*	0,53	*0,80*	0,52	*0,50*	0,54	*0,43*	0,50	*0,44*

Table 2 Calculations of structural formulae of some illitic minerals at various depths in GRT-2 well. n.a.: number of analyses; An. Av.: analytical average; s.d.: standard deviation; OCT: octahedral occupancy; INTCH: interlayer charge; XFe: Fe/(Fe+Mg).

Samples	GRT-2 2770		GRT-2 2773		GRT-2 2794		GRT-2 2950		GRT-2 2977		GRT-2 3052	
n. a.	21		15		18		29		24		20	
	An. Av.	s.d.	An. Av.	s.d.	An. Av.	s.d.	An. Av.	s.d.	An. Av.	s.d.	An. Av.	s.d.
Si	3,32	0,15	3,31	0,09	3,35	0,03	3,32	0,01	3,33	0,02	3,35	0,00
Al IV	0,68	0,15	0,69	0,09	0,65	0,03	0,68	0,01	0,67	0,02	0,65	0,00
Al VI	1,62	0,20	1,64	0,05	1,59	0,07	1,68	0,03	1,68	0,04	1,60	0,02
Fe 3+	0,17	0,08	0,17	0,01	0,19	0,02	0,15	0,03	0,15	0,05	0,19	0,02
Mg	0,18	0,11	0,18	0,04	0,20	0,06	0,15	0,01	0,15	0,01	0,19	0,04
Ti	0,00	0,01	0,01	0,00	0,00	0,00	0,00	0,00	0,00	0,00	0,00	0,00
Mn	0,00	0,00	0,00	0,00	0,00	0,00	0,00	0,00	0,00	0,00	0,00	0,00
OCT	1,99	0,01	1,99	0,00	1,98	0,01	1,99	0,01	1,99	0,00	1,98	0,00
Ca	0,00	0,00	0,00	0,00	0,00	0,00	0,00	0,00	0,00	0,00	0,01	0,00
Na	0,00	0,00	0,00	0,00	0,00	0,00	0,00	0,00	0,00	0,00	0,00	0,00
K	0,90	0,02	0,89	0,04	0,89	0,01	0,86	0,00	0,84	0,02	0,87	0,03
INTCH	0,91	0,02	0,89	0,04	0,90	0,01	0,87	0,00	0,85	0,01	0,88	0,04
XFe	0,49	0,42	0,49	0,20	0,49	0,25	0,50	0,75	0,50	0,83	0,50	0,33

Table 3 Calculations of structural formulae of some chlorite at various depths in GRT-1 and GRT-2 wells. n.a.: number of analyses; An Av: analytical average; s.d.: standard deviation; OCT: octahedral occupancy; INTCH: interlayer charge; XFe: Fe/(Fe+Mg); an. loc.: microsite of crystallization; Fe–Mg: chlorite in replacement of primary ferromagnesian minerals; FZ: chlorite crystallized in fracture zone.

Samples	GRT-1 2212		GRT-1 2368		GRT-1 2503		GRT-2 2770		GRT-2 2773		GRT-2 2773	
an. loc.	FZ		FZ		FeMg		FeMg		FeMg		FZ	
n. a.	7		10		6		2		3		4	
	An. Av.	s.d.	An. Av.	s.d.	An. Av.	s.d.	An. Av.	s.d.	An. Av.	s.d.	An. Av.	s.d.
Si	2,81	0,03	2,81	0,04	3,07	0,10	2,88	0,01	2,88	0,05	2,84	0,07
Al IV	1,19	0,03	1,19	0,04	0,93	0,10	1,12	0,01	1,12	0,05	1,16	0,07
Al VI	1,24	0,04	1,28	0,04	1,22	0,06	1,22	0,01	1,76	0,10	1,68	0,13
Ti	0,00	0,00	0,01	0,01	0,03	0,05	0,01	0,00	0,00	0,00	0,00	0,01
Fe 2+	3,77	0,24	3,81	0,25	1,70	0,16	2,01	0,12	2,18	0,12	3,67	0,32
Mn 2+	0,01	0,00	0,01	0,00	0,07	0,04	0,04	0,04	0,04	0,02	0,01	0,01
Mg 2+	0,92	0,20	0,79	0,23	2,78	0,09	2,65	0,05	2,39	0,15	0,91	0,18
OCT	5,94	0,04	5,90	0,05	5,80	0,08	5,93	0,01	5,90	0,03	5,90	0,03
Ca	0,02	0,02	0,04	0,07	0,01	0,01	0,00	0,01	0,00	0,00	0,01	0,02
Na	0,00	0,00	0,00	0,00	0,00	0,00	0,00	0,00	0,00	0,00	0,00	0,00
K	0,01	0,01	0,02	0,01	0,04	0,04	0,01	0,00	0,00	0,00	0,01	0,01
INTCH	0,05	0,04	0,11	0,14	0,05	0,04	0,01	0,01	0,01	0,00	0,04	0,02
XFe	0,80	0,04	0,83	0,05	0,38	0,03	0,43	0,02	0,48	0,03	0,80	0,05

Samples	GRT2 2794	GRT-2 2950		GRT-2 2950		GRT-2 2977		GRT-2 3052	
an. loc.	FZ	FeMg		FZ		FeMg		FeMg	
n. a.	1	2		2		5		7	
		An. Av.	s.d.	An. Av.	s.d.	An. Av.	s.d.	An. Av.	s.d.
Si	2,81	2,97	0,05	2,90	0,04	3,00	0,09	2,90	0,01
Al IV	1,19	1,03	0,05	1,10	0,04	1,00	0,09	1,10	0,01
Al VI	1,37	1,15	0,07	1,30	0,07	1,21	0,02	1,20	0,05
Ti	0,01	0,01	0,00	0,01	0,00	0,01	0,01	0,01	0,00
Fe 2+	3,13	1,97	0,16	2,92	0,08	1,92	0,07	2,01	0,11
Mn 2+	0,01	0,05	0,03	0,01	0,00	0,07	0,00	0,05	0,04
Mg 2+	1,35	2,74	0,22	1,62	0,05	2,65	0,02	2,67	0,01
OCT	5,87	5,92	0,02	5,86	0,07	5,87	0,07	5,93	0,03
Ca	0,03	0,01	0,00	0,02	0,01	0,01	0,00	0,01	0,01
Na	0,00	0,00	0,00	0,00	0,00	0,00	0,00	0,00	0,00
K	0,00	0,00	0,00	0,02	0,02	0,03	0,04	0,01	0,00
INTCH	0,06	0,02	0,00	0,06	0,04	0,04	0,05	0,02	0,01
XFe	0,70	0,42	0,04	0,64	0,00	0,42	0,01	0,43	0,01